Characterizing the Role of Syntaxin 1A in the Heart

Manvir Virdi

A THESIS SUBMITTED TO

THE FACULTY OF GRADUATE STUDIES

IN PARTIAL FULLFILLMENT OF THE REQUIRMENTS

FOR THE DEGREE OF

MASTER OF SCIENCE

GRADUATE PROGRAM IN BIOLOGY

YORK UNIVERSITY

TORONTO, ONTARIO

OCTOBER 2019

Abstract

The SNARE protein, STX1A, is expressed in various tissues. However, the role of STX1A in the heart remains unclear. Using a cardiac-specific STX1A knockout mouse model, this thesis explores the potential role of STX1A in excitation-contraction coupling. Echocardiography showed STX1A KO mice underwent transient systolic dysfunction persisting for 3 weeks. Ejection fraction and fractional shortening decreased in STX1A KO mice which returned to control levels by the 3rd week. No changes were observed in the control groups. Hypertrophy in STX1A KO hearts was not observed. Invasive hemodynamics revealed no change in LV or aortic pressures. Rate of pressure generation and relaxation were reduced in STX1A KO hearts at 0 weeks. Echocardiography also showed significant delay between the R-wave and onset of contraction in STX1A KO mice when compared to control mice. The observations of this study are indicative of STX1A's role in the maintenance of normal excitation-contraction coupling in cardiomyocytes.

Acknowledgments

My journey through graduate school has been challenging yet rewarding. I would like to take this opportunity to thank everyone that has helped me over the years or have contributed to the work presented in this thesis. You are all much appreciated. I would like to particularly thank my supervisor, Dr. Robert G. Tsushima, who has been an excellent mentor. Not only did Dr. Tsushima help expand my knowledge of cardiac physiology but has also helped me grow as an individual. It's through his guidance that I write this thesis. I would also like to extend my appreciation to Dr. Peter H. Backx, my committee member, for his invaluable input and suggestions over the years. I would also like to extend my heart filled gratitude to Xiaodong Gao, a laboratory technician in the Backx's lab, who has patiently taught me and assisted in many of the experiments presented in this thesis. During my first week of graduate school, Xiaodong Gao told me "In the lab, I am your mother and you do as I say". Being my mother in the lab she has always been a valuable resource and support during repeatedly failing experiments and the time staking efforts of trouble shooting which followed. I would also like to thank Nazar Polidovitch, from the Backx's lab, for teaching me how to perform echocardiography, retrograde heart perfusion, and for his continued assistance, guidance, and support as a colleague and friend. Nazar also, very generously, performed invasive hemodynamics data collection for this thesis. I would also like to thank Dr. Magdalena for her invaluable assistance in using the confocal microscope. This section would remain incomplete without the recognition of my fellow lab mates, particularly Amanvir Virdi, Dan Gheorghiu, and Janine Samantha Co, whom have always offered their help and support during my graduate experience. Finally, I would like to thank my parents for their continued support and for helping me get this far in life. Thank you all for making this journey one of my most-cherished memories.

Table of Contents

List of Tables

List of Figures

List of Abbreviations

ANF/P – atrial natriuretic factor/peptide

ATP – adenosine triphosphate

BNF/P – brain natriuretic factor/peptide

bp – basepair

BSA – bovine serum albumin

cGMP – cyclic guanosine monophosphate

CO – cardiac output

DAPI - 4′,6-diamidino-2-phenylindole

DNA - deoxyribonucleic acid

dP/dt – rate of pressure change

Ds/d – systolic/diastolic dimension

EC – excitation-contraction

ECG – electrocardiogram

EDTA - Ethylenediaminetetraacetic acid

EF – ejection fraction

ER-α – estrogen receptor α

FS – fractional shortening

GAPDH - glyceraldehyde 3-phosphate dehydrogenase

GSK-3β - glycogen synthase kinase 3 beta

HR – heart rate

HW/TL – heart weight/tibia length

IHC - immunohistochemistry

IVS – interventricular septum

kDa – kilo Dalton

KO – knockout

LV – left ventricle

List of Abbreviations

LVPs/d – systolic/diastole left ventricle pressure

MerCreMer (MCM) – Mutated estrogen receptor-Cre-recombinase-mutated estrogen receptor

MHC – myosin heavy chain

NCX – sodium-calcium exchanger

PBS – phosphate buffered saline

PCR – polymerase chain reaction

PFA – paraformaldehyde

RCF – relative centrifugal force

RyR – ryanodine receptor

s/dAoP – systolic/diastolic aortic pressure

SDS - sodium dodecyl sulfate

SEM – standard error of the mean

SERCA – sarco/endoplasmic reticulum Ca^{2+}-ATPase

siRNA – small interfering ribonucleic acid

SNAP – synaptosomal associated protein

SNARE – Soluble N-ethylmaleimide-sensitive factor activating protein receptor

STX – syntaxin

SV – stroke volume

SYN1 – synapsin 1

synprint – synaptic protein interaction

TBS/-T – Tri-buffered saline /- tween

VAMP – vesicle-associated membrane protein

VGCC – voltage-gated calcium channel

VGNC – voltage-gated sodium channel

Vs/d – systolic/diastolic volume

WT – wild-type

Chapter One: Introduction

1.1 Excitation-Contraction Coupling in Cardiac Myocytes

The field of cardiac research is one that has been explored for numerous centuries. The heart, by 18th century physicians, was not accredited for its role at the time. The commonly known role for the heart as a contractile organ which functions to pump blood through the closed circulatory system was not established until the observations of William Harvey in his publication "de Motu Cordis et Sanguinis in Animalibus" in 1628 (Ribatti 2009, Silverman 2007). Being the first organ to develop and the last to function in an animal illustrates the heart's true complexity and importance, which researchers and physicians today have come to appreciate (Lien et al. 1999, Olson et al. 2006). For the heart to perform its vital role in circulating blood, the heart must contract in a precise and timely manner in response to an electrical signal (Santana et al., 2010). The heart achieves this by a process referred to as excitation-contraction (EC) coupling, as illustrated in Figure 1. EC coupling consists of a series of events which convert the electrical input to mechanical energy in the form of myocyte contraction (Santana et al., 2010).

The initiation of muscular contraction requires a stimulus. In the case of the heart, this stimulus originates from the muscle itself (myogenic) from the sinoatrial node, commonly referred to as the pacemaker (Cheng et al. 1993). Shortly after the arrival of an initial stimulus, voltage-gated sodium channels open and causes a depolarization of the cardiac myocytes in phase 0 of the action potential. During phase 1 of the cardiac action potential, transiently outward potassium channels and sodium/calcium exchangers cause a small repolarising event. In phase 2, also referred to as the plateau phase, voltage-gated L-type calcium channels open allowing for an influx of calcium ions into the cardiac myocyte (Bers 2002; Cheng et al. 1993).

This initial influx of calcium referred to as a ‘spark’ then binds to and opens calcium channels on the sarcoplasmic reticulum known as ryanodine receptors (Cheng et al. 1993). This then leads to an efflux of stored calcium ions from the sarcoplasmic reticulum out to the sarcoplasm, adding significantly to the intracellular levels of calcium (Bers 2002; Cheng et al. 1993). This phenomenon is commonly referred to as calcium gain through calcium-induced calcium release. This increased release of sarcoplasmic calcium causes the myofilament protein, troponin C, to be bound by calcium, inducing a conformational change in its structure (Layland et al. 2005). The troponin complex is comprised of three different troponins (I, T, and C) subunits which are bound to the actin filament and function to inhibit the interaction between the myosin thick filament and the actin thin filament (the contractile machinery) (Layland et al. 2005). The inhibition of this interaction prevents myosin from hydrolyzing adenosine triphosphate (ATP) in order to undergo cross-bridge circling, leading to uncoordinated muscular contraction (Stephens 1965). Once a calcium-induced conformational change in troponins has occurred, it causes a relocation of tropomyosin and forces tropomyosin into a groove on the thin filament. Tropomyosin, a helical structure, is found on the thin filament which functions to hide the myosin binding sites on the actin monomers also preventing their association and unwanted contractions (Layland et al. 2005, Perry 2001). When tropomyosin is displaced, the myosin-actin binding sites are exposed allowing for myosin heads to bind and begin their motor protein function by binding to and walking along the thin filament at the expense of ATP (Barany 1967). This action of myosin is what pulls the ends of the sarcomeres in towards one another leading to their shortening which causes the shortening of the entire muscle at the macroscopic level. Muscle relaxation is also influenced by the sarcoplasmic reticular calcium levels (Asahi et al. 2004). Once contraction is completed, in phase 3 of the cardiac action potential, the reduction of

calcium influx and increase in hyperpolarizing potassium currents return the myocyte to a diastolic membrane potential (Santana et al., 2010). The calcium from the sarcoplasm is transported back into the sarcoplasmic reticulum by SERCA2 (sarco/endoplasmic reticulum Ca^{2+}ATPase) leading to a reduction in sarcoplasmic calcium levels (Asahi et al. 2004). This then allows the troponins and tropomyosin to return to their original conformations and separate the myosin-actin interaction, allowing the myocytes to relax and return to their original length (Asahi et al. 2004; Santana et al., 2010). The events between sarcolemmal depolarization to calcium release and muscular contraction are collectively known as excitation-contraction (EC) coupling.

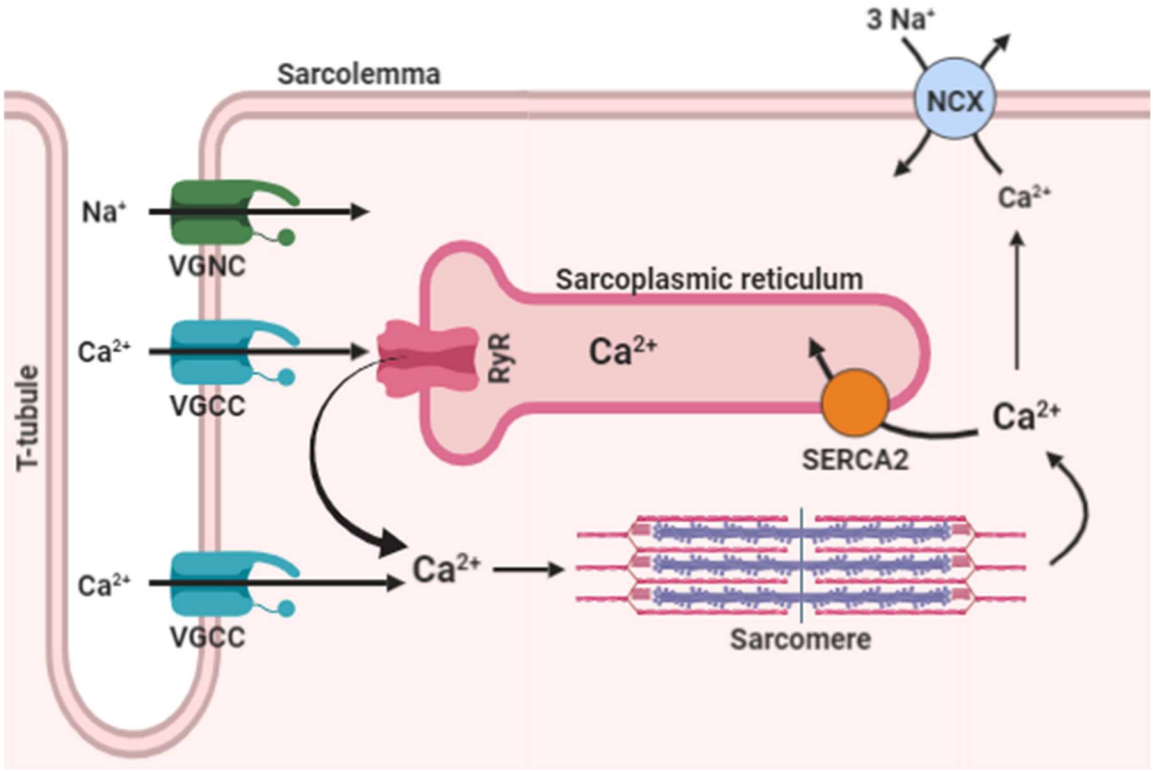

Figure 1: Excitation-contraction coupling in a cardiomyocyte. Upon a depolarizing event by voltage-gated sodium channels (VGNC), voltage-gated calcium channels (VGCC) open allowing for an influx of calcium. This calcium then binds to and opens ryanodine receptors (RyR) on the sarcoplasmic reticulum a process known as calcium-induced calcium release. Elevated cytosolic calcium levels then allow sarcomeric actin-myosin cross-bridge cycling resulting in muscular contraction. Following the contraction, cytosolic calcium levels return to basal levels through the actions of sarco/endoplasmic reticulum Ca^{2+}-ATPase 2 (SERCA2) and sodium-calcium exchanger (NCX). Figure was generated using BioRender.com.

1.2 The Heart as an Endocrine Organ

This vital role of the heart in circulating blood frequently overshadows the endocrine aspect of this organ (McGrath et al. 2005, Rubattu et al. 2004). The endocrine function of the heart was observed by the Canadian researcher, de Bold, and his team in 1981who first discovered a substance which was later isolated, sequenced, and named atrial natriuretic factor (ANF), now commonly referred to as atrial natriuretic peptide (ANP) (Seidah et al. 1984, de Bold et al. 1981). In a previous study, de Bold and colleagues (1978) found mammalian atrial

cardiac myocytes to possess a highly developed Golgi complex unlike that observed in the ventricular myocytes. A greater proportion of rough endoplasmic reticulum and membrane-bound storage granules were also seen in atrial muscle as compared to ventricular muscle. Upon morphological and histological comparisons, the granules observed in the atrial myocytes were concluded to resemble granules found in cells responsible for peptide hormone synthesis and secretion, warranting further investigation (de Bold et al. 1978). Using anesthetised rats as their model, de Bold and colleagues (1981) observed a 30-fold increase in sodium and chloride excretion through the urine in response to an atrial muscle homogenate injection. An increase in urine volume by 10-folds was also noted and that levels of potassium excretion had also doubled. Such effects were not seen when a similar injection of homogenized ventricle cardiac myocytes or of the homogenization medium were used – this supported the conclusion that atrial cells produce a potent inhibitor of renal tubular sodium chloride reuptake as no change in glomerular filtration rates between treatments was noted. However, in a later study by Bloch and colleagues in 1986, ANP synthesis and secretion was also observed from neonatal atrial and ventricular cardiomyocytes. It was concluded that the cellular mechanisms governing the production and release of this peptide hormone differ between these two cell types. Although both neonatal myocytes secrete ANP, only atrial cells demonstrate the ability to store this peptide in secretory granules while ventricular cells lack these storage granules and ANP is rapidly secreted following synthesis. From this, Bloch and colleagues (1986) concluded that neonatal atrial and ventricular ANP undergoes constitutive secretion independent of any stimuli while atrial ANP can also undergo regulated secretion in response to a stimulus. It was also noted that shortly after birth (1 week) ANP transcription from the mature ventricular myocytes was lost. In addition to

producing and secreting ANP in their neonatal stage, mature ventricular myocytes have been found to synthesize and release brain natriuretic peptide/factor (BNP/F) (McGrath et al. 2005).

Although ANP and BNP are secreted from different cell types, they have very similar biological targets which play a cardioprotective role (McGrath et al. 2005). Both hormones are involved in regulating pathways that increase blood volume and/or blood pressure (McGrath et al. 2005). This is achieved through the activation of membrane-bound guanylyl-cyclase receptors resulting in elevated levels of intracellular cyclic guanosine monophosphate (cGMP). This in turn alters the activities of other cGMP-sensitive enzymes and ion channels. One system which ANP has been found to regulate is the renin-angiotensin system (McGrath et al. 2005, Yue et al. 2000). In this system renin is released into circulation from the juxtaglomerular apparatus in response to a decline in blood pressure (McGrath et al. 2005, Wilkins et al. 1997). Renin, once in circulation, then initiates a series of cascade of events that result in the conversion of angiotensinogen to angiotensin I, which is then converted to angiotensin II. This active peptide then acts as a vasoconstrictor, helping to increase blood pressure. Angiotensin II also stimulates the secretion of a second peptide hormone from the adrenal glands known as aldosterone. Aldosterone acts to increase sodium reuptake in the distal tubule which then increases water retention, acting to increase blood volume and as a result increase blood pressure (Petty et al. 1981). ANP released in response to the activation of stretch receptors in the atria due to increased atrial preload (high blood pressure) functions to counter the renin-angiotensin system (McGrath et al. 2005, Stephenson 1990). ANP achieves this through vasodilation, increasing glomerular filtration rate, along with increasing sodium excretion in the proximal tubule (Axelsson et al. 2011, Brown and Corr 1987, Cuocolo et al. 1991). These combined actions reduce blood volume in turn reducing blood pressure.

Past studies have helped to further expand our knowledge on the heart as an endocrine organ making it more than just a rhythmically contracting muscle responsible for pumping blood. This property of the heart and the storage, temporal/regulated release, and contr ol displayed by ANP and BNP would not have been made possible without a very important class of proteins referred to as soluble N-ethylmaleimide-sensitive factor activating protein receptor proteins (Peters et al. 2006, Ferlito et al. 2010).

1.3 The Role of SNAREs in Exocytosis

Soluble N-ethylmaleimide-sensitive factor activating protein receptor proteins, commonly known as SNARE proteins, have been in the research community's spotlight for many years. Since the discovery of SNAREs in the 1990s, they have become an extensively studied protein super family (Duman and Forte 2003, Rothman 1994, Ungar and Hughson 2003). This class of proteins have become known for their role in protein trafficking/localization and membrane fusion, particularly between that of a secretory vesicle and the plasma membrane of the secretory cell, however, this is not always the case (Seino and Shibasaki 2005). Initially SNAREs were categorized using a target and vesicle naming system in which SNARE proteins located on secretory granules (vesicles) would be grouped into the v-SNARE category while those located on target membranes such as the plasma membrane would be labelled as t-SNAREs (Fasshauer et al. 1998, Jahn and Scheller 2006). This naming system fell short when classifying SNAREs involved in the fusion of two vesicles thus, a new 'Q- and R-', system has been employed. This system categorizes SNAREs based on the main amino acid in that particular SNARE motif which contributes to the central ionic layer. Q-SNAREs include those

proteins that contribute a glutamine (Q) residue while R-SNAREs are those that contribute an arginine (R) residue (Fasshauer et al 1998). In this thesis, the previous categorizing system will be used when distinguishing between the two classes.

The fusion of two lipid bilayers, structures at their lowest energy configuration and thermodynamically stable form, is an event which requires the investment of energy (Grafmuller et al. 2009). Since the vesicle membrane and plasma membrane both carry a negative net charge, electrostatic forces also hinder the fusion of these structures requiring SNARE proteins to physically overcome these barriers of exocytosis (Seino and Shibasaki 2005, Weber et al 1998). The mechanism as to how SNARE proteins achieve this has been well documented in neurons, specifically axon terminals, through studies on SNARE complexes consisting of syntaxin, synaptosomal associated protein – 25 (SNAP-25), and vesicle-associated membrane protein (VAMP) also known as synaptobrevin (Chen and Scheller 2001). Just beneath the pre-synaptic membrane, vesicles carrying neurotransmitters arrive from the Golgi. Upon arrival, the SNARE proteins, syntaxin 1A (STX1A) and SNAP-25, located on the target membrane (t-SNAREs) interact with VAMP, a v-SNARE, forming a heterotrimeric complex (Brose 2014). These interactions allow for docking of the vesicle to the inner leaflet of the plasma membrane. Membrane fusion between these two structures is initiated by a localized influx of calcium ions via voltage-gated calcium channels (Giraudo et al. 2006). This localized increase in calcium ions is detected by a protein located on the vesicle called synaptotagmin, resulting in a conformational change in the SNARE complex (Giraudo et al. 2006). The trans-SNARE complex then physically pulls together the two membranes leading to their fusion and the release of the vesicle contents (Brose 2014). This entire process is visualized in Figure 2.

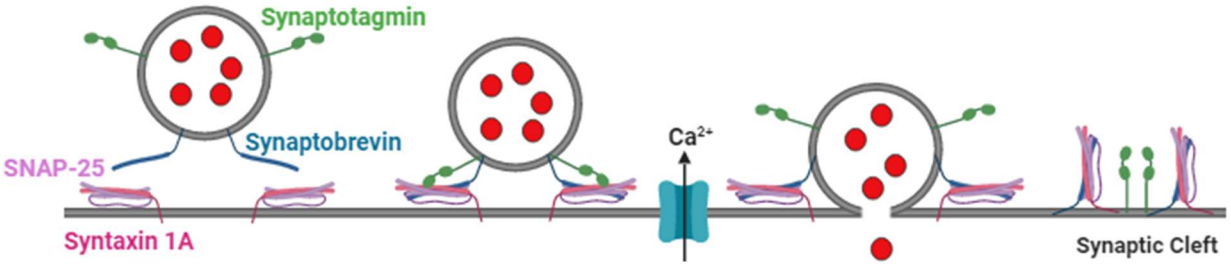

Figure 2: Illustration of SNARE-mediated exocytosis at an axon terminal. A syntaxin 1A - SNAP-25 heterodimer interacts with the v-SNARE synaptobrevin forming a trans-SNARE complex. A localized increase in cytosolic calcium via voltage-gated calcium channels is detected by synaptotagmin inducing a conformation change from trans- to cis-SNARE complex. In this process, the two membranes are pulled together. Figure was generated using BioRender.com.

Given the physiology of the nervous system and the use of chemical messengers, SNARE proteins such as STX1A, syntaxin-4 (STX4), SNAP-23, SNAP-25, VAMP -1, and VAMP-2 are highly abundant in nervous tissues (Rothman 1994). The aforementioned SNARE proteins have also been found to exhibit very specific binding with other SNARE proteins (Scales et al. 2000). It has been established that STX4 interacts with SNAP-23 forming a heterodimer on the inner leaflet of the plasma membrane which would then interact with a vesicle carrying VAMP-2. Similarly, STX1A has been shown to form a heterodimer with SNAP-25 which then interacts with a vesicle carrying either VAMP-1 or 2 (Rothman 1994). Differences in spatial expression and interactive specificity of SNAREs allows them to deliver vesicles and in turn their “cargo” to particular areas within, outside, and to the surface of the cell (Gerst 1999).

1.4 SNARE Proteins in the Heart

Aside from being highly abundant and vital for neuronal function, SNAREs can be found in various other cell types throughout the body. SNAREs have also been documented in the

heart, specifically the myocytes (Peters et al. 2006). STX1A or STX4, SNAP-23/25, and VAMP-1/2 have been found to be expressed in the adult rat heart (Peters et al. 2006). Keeping in mind that the heart is also a secretory organ, one can predict the role of SNARE proteins in the respective organ with a high degree of confidence (Seidah et al. 1984, Weber et al. 1998). The role of SNARE proteins in the exocytosis of hormones from the heart such as ANP became clearer with the observations of secretory granules containing ANP and the co-immunoprecipitation of VAMP-2, synaptogtamin, STX1, and SNAP25 complexed with ANP granules (Peters et al. 2006). Further, small interfering-ribonucleic acid (siRNA) knockdown of these SNARE proteins has allowed researchers to link select SNAREs to their traditional role as mediators of exocytosis in the heart as well (Ferlito et al 2010). In a study by Ferlito and colleagues (2010), it was demonstrated using a primary cell culture of neonatal rat cardiac myocytes that syntaxin-4, VAMP-1, and VAMP-2 are absolutely necessary for the secretion of ANP. With the use of siRNAs, these researchers were able to selectively knockout specific SNARE proteins and notice a loss in ANP secretion leading to the conclusion that the previously mentioned t-SNAREs are directly involved in the exocytosis of ANP-containing granules from cardiac myocytes. Unfortunately, the story of STX1A is not as simple and straight forward because not much is known of its function in cardiomyocytes. It is interestingly observed that the expression of STX1A and SNAP-25, two t-SNAREs, are not seen until adulthood as western blot data show no protein products in neonatal rat atrial myocytes (Peters et al. 2006). This brings into question the totality of the role these proteins have been established to perform, warranting this thesis.

1.5 Interaction of Syntaxin 1A with Voltage-Gated Calcium Channels

The role of SNARE proteins in the heart has been found to be of higher complexity than previously thought. Aside from their classical function in targeting, docking, and fusion, they have also been found to interact with various ion channels such as voltage-gated calcium channels (Wiser et al. 1996, 2002). The physical coupling of SNARE proteins with ion channels results in changes to ion currents and channel gating (Chao et al. 2011). Wiser and colleagues (1996) reported STX1A to inhibit voltage-gated calcium channels using *Xenopus* oocytes (Figure 3). It was concluded that in the absence of STX1A there were increased currents through the voltage-gated L-type calcium channels at all tested potentials (Wiser et al. 1996). Up to a 60% current inhibition by STX1A was determined. These observations remained the same with the co-expression of SNAP-25 and STX1A, however, no inhibition was noted by SNAP-25 alone (Wiser et al. 1996).

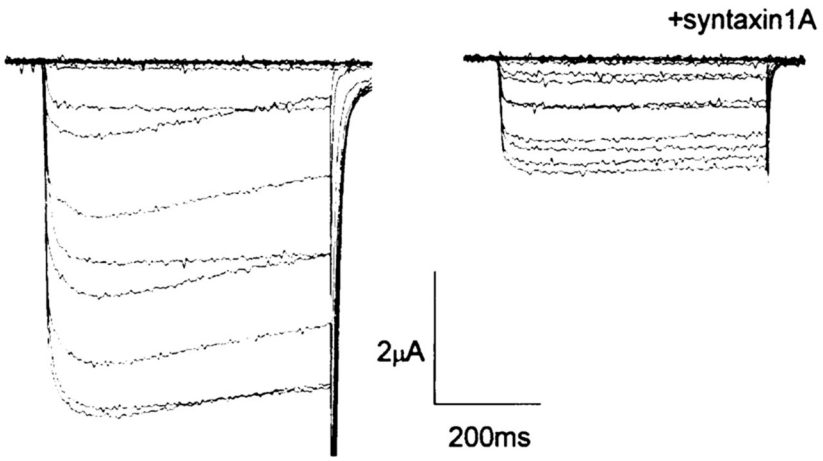

Figure 3: Inward current inhibition in the presence and absence of syntaxin 1A. Experiments were done in *Xenopus* oocytes at various test potentials from a holding potential of -80 mV. Image from Wiser et al. (1996). Copyright permission granted by The EMBO Journal.

Using a similar *Xenopus* oocyte model, STX1A monomers were demonstrated to influence voltage-gated L-type calcium channel kinetics (Arien et al. 2003). It was found that mutating cysteine-271 and cysteine-272 in the tail-anchoring helix (transmembrane domain) of STX1A to valine abolished its ability to inhibit inward Ca^{2+} currents. This mutation in STX1A also hindered its ability to form homodimers. Mutating only one cysteine to valine, however, preserves STX1A's ability to homodimerize (Arien et al. 2003). This was found to be true in the presence and absence of calcium channels. Not only was STX1A able to dimerize with one cysteine but it was also able to interact with and inhibit calcium currents through voltage-gated calcium channels such as $Ca_v1.2$ (Arien et al. 2003). It is believed that using cysteine-271 and cysteine-272, via disulfide bonds, STX1A can interact with other proteins or other STX1A molecules. Cleavage of cytosolic regions by botulinum toxin C1 also demonstrated impaired channel inhibition by STX1A (Arien et al. 2003). This allowed the conclusion that both transmembrane cysteines and cytosolic domains of STX1A are required to inhibit Ca^{2+}current through voltage-gated calcium channel $Ca_v1.2$ (Arien et al. 2003; Figure 4). It was concluded

that the direct site of action by STX1A is the $\alpha_1$1.2 pore-forming subunit to which STX1A binds to at two sites; the transmembrane region and cytosolic region (Arien et al. 2003). The cytosolic region at which STX1A binds to the α_1 subunit is referred to as the synaptic protein interaction (synprint) site, a large intercellular loop located between domains II and III (Sheng et al. 1996; Watanabe et al. 2010). In a later study by Xie et al. (2016) proposed that the cytosolic domain of STX1A, however is able to interact with voltage-gated calcium channels, it may not be responsible for inhibiting currents through these channels but rather adding preference to which calcium channel STX1A binds. More research is needed to determine which is truly the case.

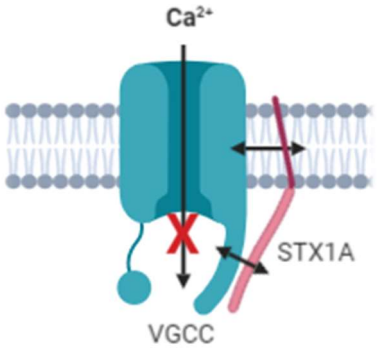

Figure 4: Model illustrating possible syntaxin 1A and VGCC interactions. This is achieved via the transmembrane and cytosolic domains. Syntaxin 1A interacts with voltage-gated calcium channels at the α-pore-forming subunit at two locations, one being in the transmembrane region and the other at the cytosolic synprint site. Syntaxin 1A is believed to carry out this interaction using cysteine-271 and -272 via disulfide bonds. Figure was generated using BioRender.com.

A concentration dependent relationship between STX1A and degree of channel inhibition was also observed allowing the authors to propose possible cooperative binding and inhibition by STX1A (Figure 5).

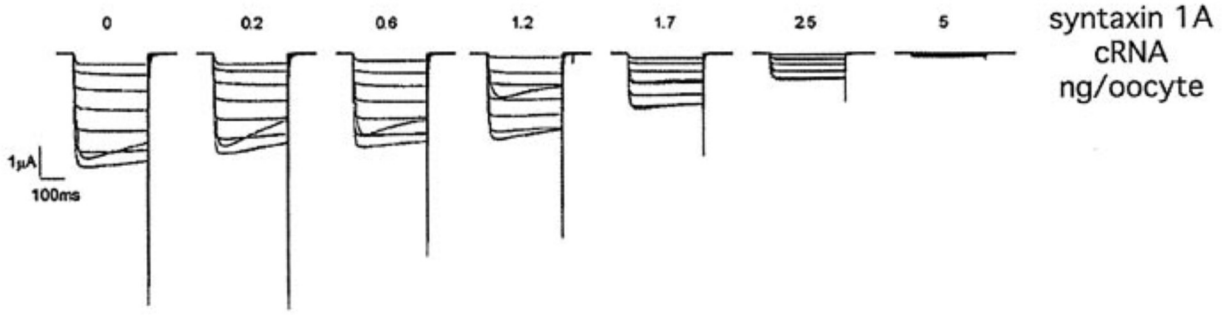

Figure 5: Syntaxin 1A cRNA concentration dependent inhibition of calcium currents. The figure shows reduced L-type calcium currents in response to 300-ms test pulse from a -80 mV holding potential. Image from Arien et al. (2003).

In an investigation by Toft-Bertelsen and team (2016), they concluded that SNAP-25 directly does not inhibit voltage-gated Ca^{2+} currents. Its interaction with STX1A facilitates STX1A dispersal from its clusters, increasing monomer availability and current inhibition as a result. The authors extend this conclusion to other proteins which also interact with STX1A.

Considering the role these channels and calcium play in the proper generation of the cardiac action potential and contraction as discussed previously, the role and influence of SNARE proteins on the excitability and proper functioning of the heart can be deduced (Faber et al. 2007). Thus, the perception of SNARE proteins continues to amend as more is learnt about this protein super family.

1.6 Objectives and Hypothesis

The objective of my thesis is to characterize the function of STX1A in the mouse heart. Changes in contractility of heart-specific STX1A knockout mice will be assessed.

Based on the inhibitory interaction of STX1A on voltage-gated calcium channels in the heart, as discussed above, it has been predicted that positive inotropic (force of contraction generated by cardiac muscle) and chronotropic (rate of heart contractions) effects can be observed from the knock-out of STX1A. This has been predicted on the grounds that once STX1A is removed there will be an increase in calcium currents through the respective channels elevating cytosolic calcium delivered to the cardiac myocytes in a shorter period of time leading to stronger and faster contracting heart (Bers 2002, Fabiato 1983).

Chapter Two: Methods

Chemicals and reagents were purchased from Sigma-Aldrich Canada (Oakville, ON) unless specified.

2.1 Mouse Model

The transgenic C57BL/6 mice expressing Cre recombinase under the α-myosin heavy chain (MHC) promoter were provided by Dr. Jeffery Molkentin (Cincinnati Children's Hospital Medical Centre, Cincinnati, OH) (Sohal et al., 2001). These mice have restricted Cre expression in cardiac myocytes (Pugach et al., 2015; Sohal et al., 2001). The syntaxin 1A (STX1A) flox/flox C57BL/6 mice were obtained from Dr. Herbert Gaisano (University of Toronto, Toronto, ON) (Liang et al. 2016). The LoxP sites flank exon 2 and 3 of STX1A.Through crossbreeding, animals homozygotic at both loci were obtained and used in this thesis. Mice were provided normal chow diet and water *ad libitum*. Male mice between the ages of 3-4 months were used. All procedures were approved by the York University Animal Care Committee in accordance to the Canadian Council on Animal Care.

2.2 Mouse Tail Genotyping

Genomic DNA used for genotypic screening of experimental mice was isolated from tail clippings. Mice were anesthetized using isoflurane in a small closed container. Once the absence of a toe-pinch reflex was observed, animals were removed from the container and a small tail sample from the end was collected into a 1.5 Eppendorf tube. Kwik stop styptic powder was applied to the tail end to stop the bleeding and prevent wound infection. Next, 300 µL of 0.05N

NaOH was added to the tube and incubated at 95ºC for 1.5 h on a dry bath. After incubation, 0.5M Tris-HCl buffer (4.44% w/v of Tris-HCl and 2.65% w/v of Tris-base) was added to the tubes to neutralize the DNA solution. The samples were used right away or stored at -20ºC for later use. Polymerase chain reaction using the appropriate primers was performed on the isolated DNA or the DNA was stored at -20ºC for later use.

PCR amplification of the isolated DNA with the appropriate primers was conducted using 2X PCR Taq Plus Master Mix (Lot. RZ794838; Applied Biological Materials). Each reaction tube had a total volume of 20 µL consisting of 1 µM forward and reverse primers each, 10 µL of the 2X PCR Taq Plus Master Mix, 4 µL of Invitrogen ultrapure DNAse and RNAse free water, and 2 µL of isolated genomic DNA. To ensure the presence of the αMHC-MCM/STX1A flox/flox in our experimental animals, the following primers were used (Liang et al., 2016). STX1A forward: GCT GCA GAA GCA AGA GAA CC, STX1A reverse: CAG CCA TAC AAA AAC CAC CA. The PCR protocol for STX1A primers was as follows: activation of polymerase at 95 °C for 5 min, 34 cycles of 95 °C for 30 sec, 60°C for 30 sec, and 72 °C for 30 sec. MCM forward: CGT CCT CCT GCT GGT ATA G, MCM reverse: GTC TGA CTA GGT GTC CTT CT. The PCR protocol for MCM primers was as follows: activation of polymerase at 95 °C for 5 min, 39 cycles of 95 °C for 30 sec, 50°C for 30 sec, and 72 °C for 30 sec. The PCR products were then stored at -20ºC or resolved on an agarose gel.

PCR products were resolved on a 1.5% (w/v) agarose gel made in 0.5X Tris-acetate-EDTA (TAE; 20 mM Tris-base, 10 mM acetic acid, and 0.5 mM EDTA). After microwaving the agarose solution in intervals of 20 seconds until all agarose particulates were dissolved, the agarose was cooled at room temperature for 5 min before adding RedSafe 20,000X at 8% v/v. After allowing the agarose gel to solidify for 20 min, 10 µL of the prepared PCR samples were

loaded into each well. Samples were prepared for loading by adding 4 μL of 6X DNA loading dye (30% v/v glycerol, 0.25%w/v bromophenol blue, 0.25% w/v xylene cyanol FF) to the PCR tubes. A wild-type control was also resolved on the gel. A 100 base pair (bp) DNA ladder (ForggaBio, Toronto, ON) was resolved alongside the samples. A 100V potential was applied for 20-25 min after which the resolved samples were visualized using the Alpha Innotech Alpha Imager Hp System gel imaging system (Alpha Innotech, now part of Cell Biosciences). Exposure time was automatically optimized by the scanning software.

2.3 Tamoxifen Treatment

Tamoxifen citrate (EMD Millipore Corp. Lot #2937852) was added to peanut oil (Sigma-Aldrich Canada) in a 1.5 mL Eppendorf tube to achieve a concentration of 10 mg/mL. To dissolve the tamoxifen, the solution was vortexed 3x for 20 secs and then sonicated (10% amplitude) 2x for 30 sec while in ice. Once a homogenous mixture was achieved, tamoxifen citrate (40mg/kg) was administered to C57BL/6 STX1A flox/flox mice 3-4 months of age via an interperitoneal injection. Other C57BL/6 STX1A flox/flox mice received only a peanut oil injection (vehicle control) which was prepared in an identical manner as the tamoxifen citrate. For ease of handling, animals were lightly anesthetised in a closed container using an inhalation anesthetic (isoflurane). A total of 4 tamoxifen injections were administered to the mice over a 4-day period. Similar injection protocol was followed for GSK-3β flox/flox (Cre+) mice and wild-type mice which both received tamoxifen injections.

2.4 Heart Tissue Collection

Mice were injected interperitoneally with 1000 USP heparin (hepalean, Organon Teknika, Toronto, ON) diluted in 1X Phosphate Buffered Saline (PBS; 145 mM NaCl, 2.7 mM KCl, 8.1 mM Na_2HPO_4, and1.5 mM KH_2PO_4, pH 7.4). Following a 5 min waiting period, mice were transferred to a small closed container which contained a cotton swab soaked in isoflurane. Mice were kept in this container until no toe-pinch reflex was observed. Mice were then euthanized via cervical dislocation. A deep transthoracic incision was made below the diaphragm. The diaphragm was then cut to expose the heart. Lateral cuts to the left and right ribs were made allowing the rib cage to be lifted and held back using a hemostat. Once the pericardial sac was removed, the heart was lifted from the base and cut out of the animal. Then, the heart was placed immediately in a weigh boat containing 1X PBS to wash out any remaining blood and transferred into another weigh boat with fresh 1X PBS. Under a dissecting microscope, the atria, left ventricle free wall, and ventricular septum were isolated and placed into cryotubes on ice which were then stored at -80^{o}C.

2.5 Protein Isolation from Tissue

Frozen tissue samples were transferred to a glass homogenizer containing 400 µL of 2x sodium dodecyl sulfate (SDS) lysis buffer (13.6% 1M Tris-HCl pH 6.8, 40% of 10% SDS, 20% of 10% glycerol, 26.4% of ultrapure water, 4 mg/10mL Complete Mini EDTA-free protease inhibitor tablets). Manual homogenization was performed on ice until a homogenous solution was achieved. The lysate was then transferred to a 1.5 mL Eppendorf tube, boiled for 5 min at

100ºC in a dry bath, and then centrifuged at 13, 845 RCF for 15 min at 4ºC. The supernatant was collected and stored at -80ºC.

2.6 Bradford-Lowry Protein Assay

From a stock of 1µg/µL bovine serum albumin (BSA) solution, a serial dilution was prepared to make 60µL of 1, 0.5, 0.25, 0.125, 0.0625 µg/µL BSA standards in 1.5 mL Eppendorf tubes. To 5 of the 6 cuvettes, 20µL of the standards were added while the 6th cuvette received 20µL of ultrapure water and served as the blank. For each sample to be quantified an independent cuvette was prepared with 20µL of a 10X dilution of the stock lysate. To each cuvette, 100µL of a 50:1 mixture of reagent A and reagent S was added followed by the addition of 800µL of reagent B (in dark). The cuvettes were then gently vortexed and allowed to incubate in a closed opaque cuvette container for 20 min. Following incubation, an Eppendorf biophotometer was used to measure absorbance at 660 nm. The standard BSA values were plotted on an absorbance vs. concentration graph to generate a standard curve, which was used to interpolate the total protein concentrations of the unknown lysates.

2.7 Western Blot

Tissue lysates were diluted to the desired final concentration for loading using 20µL of 6X SDS reducing buffer (0.28M of 1M Tris-HCL pH 6.8, 30% v/v glycerol, 10% w/v SDS, 0.5M dithiothreitol, and 0.0012% w/v bromophenol blue) and the required amount of ultrapure water to bring the final volume to 100 µL. The prepared samples were then resolved on a

polyacrylamide gel which consisted of a 5% stacking layer (ultrapure water, 30% acrylamide mix, 1M Tris-HCl pH 6.8, 10% SDS, 10% ammonium persulfate, and TEMED) and an appropriate percentage running layer (ultrapure water, 30% acrylamide mix, 1.5M Tris-HCl pH 6.8, 10% SDS, 10% ammonium persulfate, and TEMED). The polyacrylamide gel was clamped to the electrophoresis apparatus and submerged into 1X running buffer (24 mM Tris-base, 180 mM glycine, and 3.4 mM SDS)**.** Excelband pm2700 protein marker and the loading samples were applied a 100V for 20-30 min until the front reached the running layer at which the voltage was increased to 150V for 1-1.5 h until the front reached the bottom of the gel. Alongside the experimental samples, appropriate positive controls were also resolved.

Upon completion of the run, the proteins in the polyacrylamide gel were transferred to a nitrocellulose membrane. A transfer sandwich was constructed in which a pre-soaked nitrocellulose membrane in transfer buffer (25mM Tris base, 192 mM glycine, and 10% methanol) was positioned onto the polyacrylamide gel ensuring no air bubbles were caught between the two. These were then tightly clamped between filter papers and sponges which were also pre-soaked in transfer buffer. The transfer sandwich was then submerged into a tank filled with transfer buffer in a manner that the polyacrylamide gel faced the negative electrode. An ice pack was placed inside the transfer tank and the entire electrophoresis apparatus was subsequently placed in an ice bath. The proteins were transferred for 2 h at 100V.

Following the 2 h transfer, the transfer sandwich was disassembled and the membrane was washed at room temperature in a clean container 3x for 5 min using 1X Tris-buffered saline with tween 20 (TBST; 2 mM Tris base, 13.7 mM NaCl, and 0.1% tween 20, pH 7.6) while rocking. The membrane was then placed in blocking solution at room temperature (5% w/v skim milk powder in TBST) for 1 h and then washed again 3x for 5 min. Primary antibodies for the

protein of interest were prepared at a ratio of 1:1000 in 1% BSA (1% w/v of BSA in TBST and 0.02% v/v of 10% NaN_3) and placed on the membrane and incubated overnight at 4ºC (Table 1). Glyceraldehyde 3-phosphate dehydrogenase (GAPDH) served as a loading control to show comparable protein was loaded in each lane. The primary antibodies were then removed and stored at 4ºC for future use and the membrane was washed again as indicated above at room temperature. Secondary antibodies were prepared at a ratio of 1:10,000 in 50:50 mixtures of 1XPBS and 1% BSA. Secondary antibody incubation was performed at room temperature for 1 h while rocking. The secondary antibody was then removed and stored at 4ºC for future use and a 15 min 1X TBST wash was performed followed by three 5 min washes. The membrane was scanned using a LI-COR odyssey infrared imaging system using the pre-set membrane parameters.

Table 1: List of antibodies used with their dilutions, host species, class, and source.

	Host/Class	Source, Cat#	Dilution
Primary Antibodies			
Anti-syntaxin 1A	Rabbit, polyclonal	Abcam, #ab70293	1:500 (IHC)
Anti-syntaxin 4	Rabbit, polyclonal	SYSY, #110 042	1:1000 (WB)
Anti-syntaxin 3	Rabbit, polyclonal	SYSY, #110 032	1:1000 (WB)
Anti-syntaxin 2	Rabbit, polyclonal	SYSY, #110 022	1:1000 (WB)
Anti-synapsin 1	Rabbit, polyclonal	Abcam, #ab8	1:1000 (WB)
Anti-Estrogen Receptor α	Mouse, monoclonal	Abcam, #ab16460	1:1000 (WB)
Anti-GAPDH	Mouse, monoclonal	Abcam, #ab8245	1:1000 (WB)
Secondary Antibodies			
Anti-Mouse	Goat, polyclonal	LI-COR, #926-32210	1:10,000 (WB)
Anti-Rabbit	Goat, polyclonal	LI-COR, #926-68071	1:10,000 (WB)
Anti-Rabbit Alexa Fluor 647	Goat, polyclonal	Thermofisher, A-21244	1:500 (IHC)

*WB = western blot. IHC= immunohistochemistry.

2.8 Paraformaldehyde Solution

Paraformaldehyde solution was prepared by adding 4% (w/v) paraformaldehyde (PFA) powder to 1X PBS. The solution was heated to 60^{o}C on a hot plate and constantly stirred to prevent boiling. Next, the pH was raised by adding 1 N NaOH in a drop wise manner until the solution became clear. Once the solution cooled to room temperature, the pH was adjusted to 7.4 using 10 N HCl after which the solution was raised to its final volume using 1x PBS. Lastly, the solution was filtered through a 40 μm filter and stored at 4^{o}C to then be used the following day.

2.9 Paraformaldehyde Heart Fixation

Mice were interperitoneally injected with 1000 USP heparin diluted in 1X PBS. Following a 5 min period, mice were euthanized via cervical dislocation. A deep transthoracic incision below the diaphragm was made. After the diaphragm was cut, two lateral cuts along the left and right ribs were made and the rib cage was then raised exposing the heart. The pericardial sac was then peeled off the heart and the inferior vena cava was cut. Following which, 5-10 mL of 1% KCl solution in 1xPBS was injected into the apex of the left ventricle until the liver and lungs became white in color. The heart was then lifted from the base and cut out of the body and immediately placed into a weigh boat containing 4% PFA for a quick wash. The heart was then cannulated with a 20-gauge cannula and perfused with 15 mL of 4% PFA using a horizontal profusion system. Profusion rate was adjusted to maintain profusion pressure of 70-80 mmHg. Hearts were then stored in 15 mL test tubes containing 4% PFA for 24 hat 4^{o}C and then transferred into 1X PBS for long term storage at 4^{o}C.

2.10 Embedding Paraformaldehyde Fixed Hearts in Paraffin

Paraformaldehyde fixed hearts were delivered to The Centre for Phenogenomic, Toronto to be embedded in paraffin wax for slicing along the frontal plane (4 chamber view).

2.11 Paraffin embedded Heart Slicing

Paraffin blocks containing the hearts to be sliced were fastened to the cryotome and 5 μm thick slices were made. These slices were then transferred on to a slide covered in 70% ethanol for inspection and then to a lukewarm water bath allowing the wax slices to expand. Once fully reopened from the slicing process, Fisherbrand Superfrost Plus microscope slides were lowered under the floating slices and slowly raised allowing the heart slices to adhere to the slides. The slides were then incubated overnight at 37^{o}C before being used.

2.12 Immunohistochemistry

For immunohistochemistry, slides were first washed twice with xylene for 5 min each followed by a 1:1 xylene-ethanol solution for another 5 min. Gradient ethanol washes were then performed for 5 min each going from two 100 % ethanol washes to 95 %, to 70 %, and finally to 50 % ethanol. The slides were then rinsed for 10 min using ultrapure water. Slides were transferred to a horizontal metal staining rack which was placed in an autoclave safe container. After lowering the container into a pressure cooker, the container was filled with antigen retrieval solution/sodium citrate buffer (10 mM sodium citrate and 0.05% Tween 20 in ultrapure water, pH 6.0). The pH was adjusting using 10 N HCl. Ultrapure water was added to the pressure

cooker in order to surround and half-way submerge the container. The lid was tightly secured, and the pressure cooker was placed on a hot plate at max heat. Samples were boiled for 3 min following the first whistle of the pressure cooker which was then placed under running cold water with the whistle raised. Then once the pressure was released, the slides were removed and washed 3x for 5 min in wash buffer consisting of 1X TBS (2 mM Tris base, 13.7 mM NaCl, pH 7.6) with 0.025% triton X-100. Samples were then blocked using 1% (w/v) BSA dissolved in 1X TBS overnight at 4^{o}C. Following blocking, the solution was discarded, and the slides were washed 3x for 5 min using wash buffer. Using a PAP pen, a circle surrounding the sample to be stained was drawn. Primary antibody for the protein of interest was diluted to a ratio of 1:500 in 1% BSA in 1X TBS with 0.5% triton X-100 (Table 1). Primary antibodies were pipetted on to the heart slices and incubated overnight at 4^{o}C followed by 3x 5 min washes with wash buffer. Secondary antibodies were diluted and applied as were the primary antibodies but incubated for only 1 h at room temperature in dark. Following another series of 3x 5 min washes, slides were mounted using Fluoroshield histology mounting medium with DAPI (Cat. F6057) and 1 mm thick cover slips. Slides were allowed to dry in the dark for 24 h before being observed using a confocal microscope.

2.13 Echocardiography

Transthoracic 2D, M-mode, echocardiographic measurements were done using VisualSonics Vevo 2011 high resolution ultrasound imaging system (FUJIFILM VisualSonics, Toronto, ON). Mice were first transferred to a clear small closed container. Employing an isoflurane vaporizer, 3% isoflurane was delivered to the container by oxygen gas (carrier gas).

Once the mice demonstrated impaired dorsal - ventral axis maintenance, they were placed on a heated electrode pad in the supine position. Electrode gel was applied to the front and hind paws and tapped securely over the electrodes. The snout of the mice was then placed into a snout cone which continuously delivered 1.5-2% isoflurane to the animal. A rectal probe, lubricated using Vaseline, was then gently inserted into the mice to monitor core body temperature. With the use of the heated pad and a heat lamp, the core body temperature of the mice was maintained between 37.2-37.4ºC. The isoflurane percentage was adjusted as needed to maintain a respiratory rate between 90-110 breathes per minute. Once the mice were setup on the electrode pad, the fur on the thorax was removed using an electric shaver followed by the application of depilatory cream (Nair^{TM}) for 30 seconds. The hair removal cream was then wiped off using a damp Kimwipe to expose the skin. Acoustic gel was then generously placed on the animal's thorax into which an ultrasound probe, mounted on a micromanipulator, was lowered. Using the long axis B-mode, the midsagittal axis of the left ventricle (LV) was located. Once the apex and base of the heart were aligned horizontally in the long axis view, short axis B-mode was used to align the papillary tendineae vertically to one another. Long axis B-mode was then used to relocate the midsagital axis of the LV and ensure the apex and base were still aligned. After allowing the mice to stabilize, the scan was saved and diastolic dimension, systolic dimension, and posterior wall thickness was measured at the widest part of the LV (greatest separation between the anterior and posterior walls). Next, the M-mode at the same region was used to monitor LV wall movement overtime. Average diastolic and systolic parameters were determined, along with fractional shortening (FS), ejection fraction (EF), stroke volume (SV), and cardiac output (CO). The values of diastolic and systolic dimensions and posterior wall thickness were then compared to those obtained from the B-mode to ensure they agreed to the nearest 1/100 of a millimeter.

Time between the peak R-wave on the ECG and the onset of contraction (first upwards movement of the left ventricular posterior wall) was also measured at three different points for each M-mode and averaged. All measurements were done using the preinstalled VisualSonics' cardiology package.

2.14 Invasive Hemodynamics

Mice were anesthetised using a 3% isoflurane oxygen mixture in a sealed container. Once the mice failed to display a toe-pinch reflex, they were transferred to a heated pad and positioned supine with the head facing towards the experimenter. Surgical suture was placed under the top front incisors to secure the snout in the snout cone which continued to deliver 3% isoflurane. An incision along the mid sagittal axis of the neck was made approximately 1 cm in length. Using blunt dissection, the musculature and submandibular glands were gently separated exposing the underlying right carotid artery. Carefully, the vagus nerve was separated from the carotid artery. Saline was periodically applied to the exposed tissue to keep it hydrated. Suture was tightly knotted around the right carotid artery mid-way and was slightly pulled distally bringing the vessel into tension. Another piece of suture was then threaded underneath the vessel and both ends were pulled towards the posterior of the animal, blocking the carotid artery at this point as well. A saline filled syringe with a 23-gauge needle was used to puncture the carotid towards the proximal end. After washing away the blood which had escaped the artery, a calibrated solid state Transonic Scisense catheter was than introduced into the vessel and the second suture was freed allowing the catheter to continue proximally into the aorta. At this time 1.5-2% isoflurane was used to keep the mice anesthetised at a respiratory rate of 90 and a core body temperature of

37.2-37.4ºC (measured via rectal probe). Aortic pressure recordings were taken until a stable trace was observed. The catheter was then advanced into the left ventricle and the same data collection process was repeated. Following the completion of the experiment, the catheter was slowly retracted out of the carotid artery and a small amount of blood was allowed to escape the vessel to flush out any debris. The carotid was then tied off at the proximal end and the distal end knot was cut from the remaining suture and left intact, relieving the tension and allowing the vessel to return to its normal position. The exposed tissue was cleaned using betadine solution (1% iodine) and the skin was then sutured together. Origin Pro (OriginLab Corporation, Northampton, United States of America) was used to collect and tabulate peak values from the pressure traces which were then exported to Excel and averaged.

2.15 Morphometry

In order to quantify possible hypertrophy, heart weight (g) was normalized to tibia length (cm). Hearts, as outlined previously, were isolated from mice. The hearts were then gently dried on paper towel after been washed in 1X PBS and weighed on a microscale. The right hind limb of the mice was severed and placed into a 15 mL tube containing bleach. After 48-72 h, the bleach was poured out leaving behind the exposed skeletal structure. Using a digital vernier caliper, the isolated tibia was measured long its frontal and sagittal planes and an average tibia length was determined.

2.16 Densitometry Analysis

Image Studio Lite was used to measure western blot band density for the protein of interest and the loading control (GAPDH). Once background was subtracted, target protein values were divided by those of the loading control and normalized to the appropriate controls. Densitometry figure was generated using Graphpad Prism 7.

2.17 Statistics Analysis

Graphpad Prism 7 was used to generate figures and perform a one-way ANOVA ($\alpha<0.05$) followed by a Tukey multiple comparisons test. P values less than 0.05 were determined to be significantly different.

Chapter Three: Results

The objective of this thesis was to characterize the function of syntaxin 1A (STX1A) in the mouse heart. Cardiac-specific STX1A knockout mice were generated by crossing C57BL/6 transgenic mice expressing Cre recombinase under the α-MHC promoter with STX1A floxed gene. Physiological and morphological changes to the mouse hearts were measured.

3.1 Conformation of transgenic STX1A flox/flox and αMHC-MCM expression

The presence of the STX1A flox/flox and αMHC-MerCreMer (MCM) in the mice were confirmed by PCR genotyping (Figures 6 and 7). STX1A flox/flox and MCM mice showed the predicted bands at 250 bp and 406 bp, respectively, which were absent in wild-type (WT) mice.

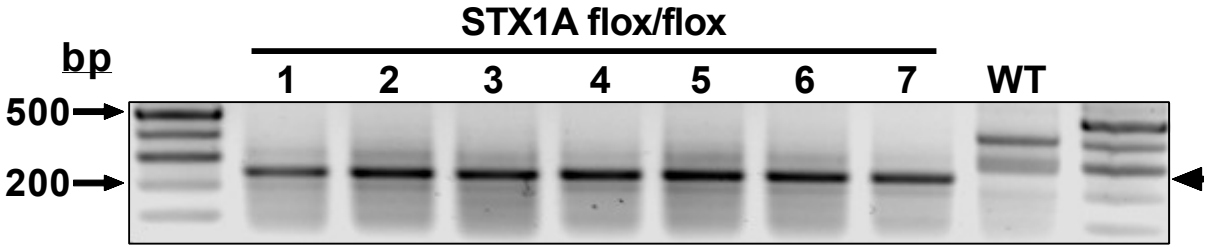

Figure 6: STX1A flox/flox genotyping using tail clips resolved on a 1.5% agarose gel. A positive result was demonstrated by a band ~250 bp in length (arrowhead) whereas the wild-type produced a band ~400bp.Agarose gel was visualized using an Alpha Imager HP gel imaging system.

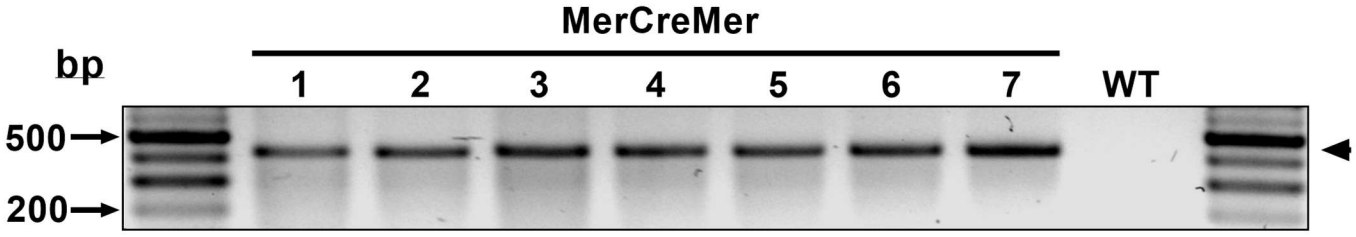

Figure 7: MCM genotyping results using tail clips resolved on a 1.5% agarose gel. A positive result was demonstrated by a band ~450 bp in length. Agarose gel was visualized using an Alpha Imager HP gel imaging system.

To further validate the expression of MCM, Western blot analysis was conducted on left ventricular tissue from wild-type and transgenic mice (Figure 8). Multiple Cre primary antibodies were used in efforts to detect the MCM protein but repeated attempts to detect Cre protein were unsuccessful. Due to the fused mutated estrogen receptor domain of MCM, estrogen receptor α (ER-α) primary antibodies have been used to detect this protein (Kam et al. 2012). Initial attempts using anti-rabbit ER-α were unsuccessful in detecting MCM or endogenous estrogen receptor. Later, an anti-mouse ER-α primary antibody was used which successfully detected the MCM protein. A 113kDa band was observed which is indicative of MCM. This band was absent in mice lacking this transgene.

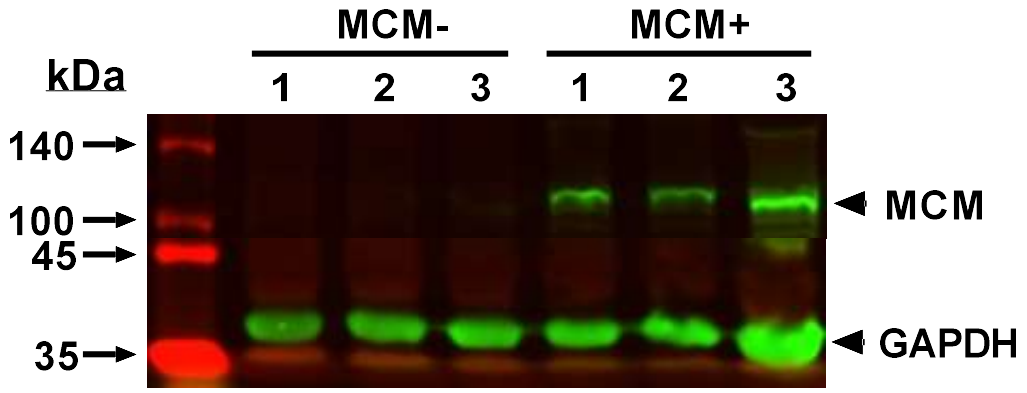

Figure 8: Western blot analysis of MCM expression in C57BL/6 left ventricles. Protein lysates from three αMHC-MCM STX1A floxed hearts and three WT C57BL/6 mice (negative control; MCM-) were resolved by SDS-PAGE. Each well contained 30 µg of protein. Mouse monoclonal antibody for estrogen receptor alpha (1:1000) was used to probe for MCM. Glyceraldehyde 3-phosphate dehydrogenase (GAPDH) served as the loading control. A positive MCM result was observed at ~110 kDa with the GAPDH band at ~37 kDa. Membranes were visualized using a LI-COR Odyssey infrared imaging system (n=3).

3.2 Confirmation of STX1A KO in αMHC-MCM/STX1A flox/flox Mice

Experiments were conducted to confirm knockout of STX1A protein in the mouse hearts. Initial Western blots were performed to verify the lack of neuronal contamination in the LV free wall and intraventricular septum (IVS) samples as this may contribute to the STX1A detection (Mishima et al. 2014). These isolated samples were probed for synapsin 1 (SYN1), a neuronal marker (De Camilli et al 1983). SYN1 was not found in either the LV free wall or IVS (Figure 9). Multiple Western blot attempts to detect STX1A protein in the wild-type and transgenic αMHC-MCM/STX1A floxed mice from LV and IVS were not conclusive. Immunohistochemistry (IHC) was used as an alternative approach to confirm successful STX1A knockout (Figure 10). Prior to tamoxifen treatment, STX1A (red) was observed on the sarcolemma of LV cardiomyocytes. The red outline and speckling pattern of STX1A seen in pre-tamoxifen heart samples is similar to what has been previously reported in neurons by Ullrich et al. (2015). STX1A expression patterns seen in pre-tamoxifen heart slices were not observed in 0 week and 3 week post-tamoxifen heart slices indicative of STX1A KO (Figure 5). DAPI (blue) was used as a DNA marker.

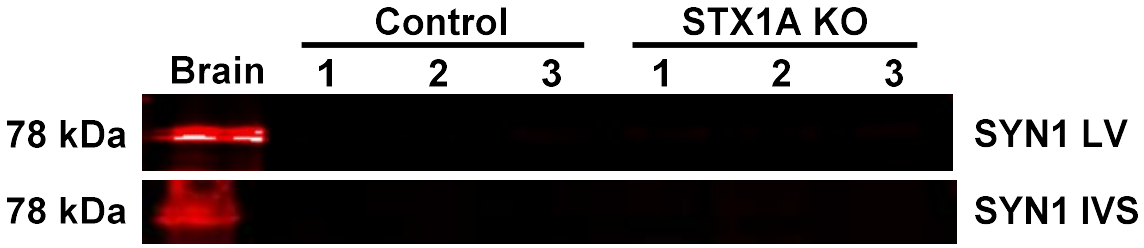

Figure 9: Western blot analysis of synapsin 1 (SYN1). Protein was isolated from LV and interventricular septa (IVS). Protein lysates from three LVs and IVSs from αMHC-MCM STX1A floxed mice injection with peanut oil (control) and those treated with tamoxifen (STX1A KO) were resolved by SDS-PAGE. Each well contained 30 µg of protein. Brain lystate (10 µg) served as a positive control for SYN1. Rabbit polyclonal antibody for synapsin 1 (1:1000) was used. A positive SYN1 result was observed at ~78kDa. A LI-COR Odyssey infrared imaging system was used to visual the membranes (n=2).

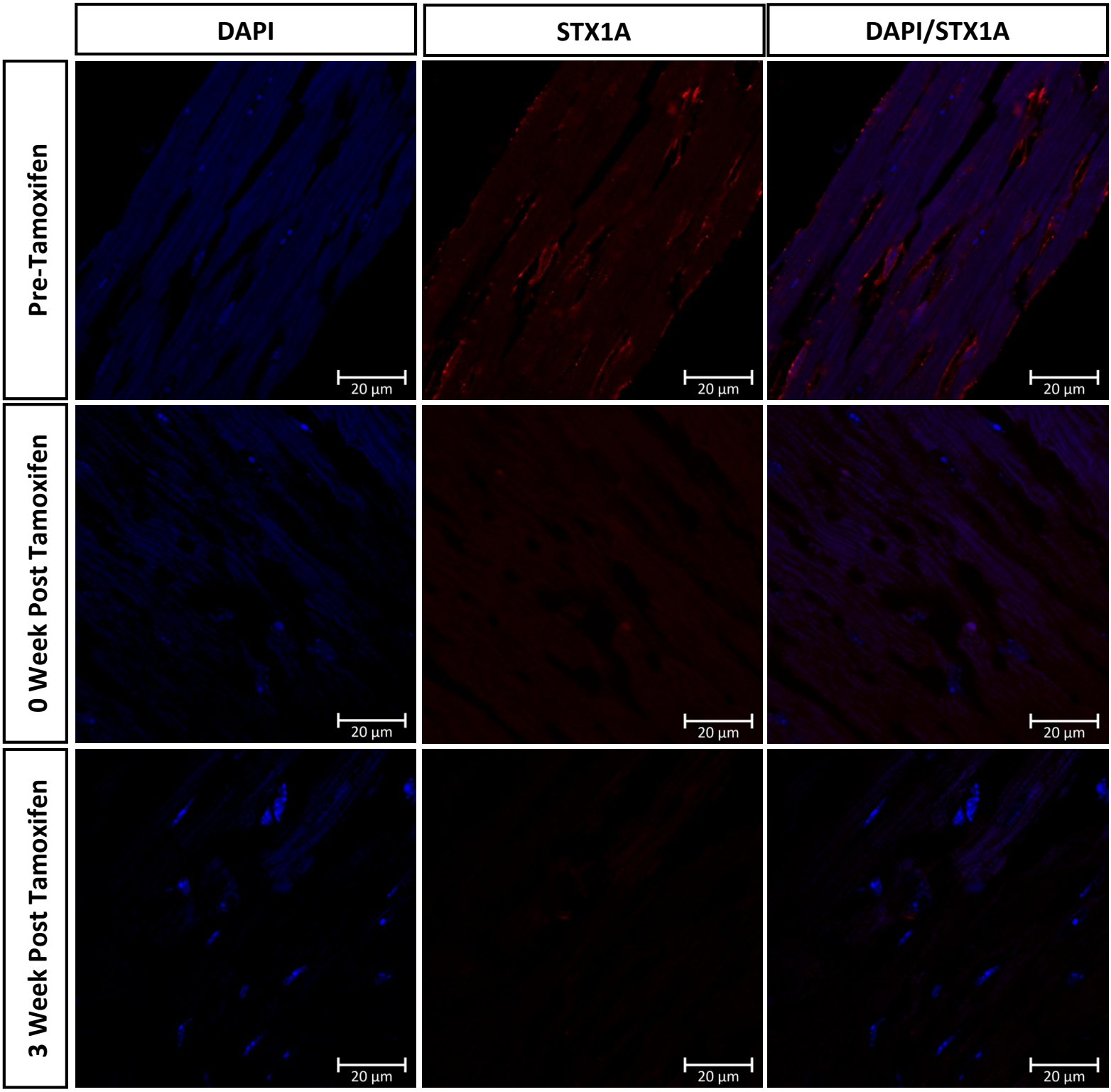

Figure 10: Immunohistochemistry of STX1A KO mice. Frontal heart slices of pre, 0 week, and 3 week post tamoxifen treatment were probed with rabbit polyclonal STX1A antibody (1:500) and secondary anti-rabbit alexafluor 647 (red; 1:500). DAPI (blue) present in the mounting medium was used as a DNA marker. Slides were visualized with a ZEISS LSM 700 confocal microscope. A 63X objective with emersion oil was used.

3.3 Heart Function of Tamoxifen-Treated and Cre-Positive Mice

To conduct longitudinal assessment of heart function in the mice, transthoracic 2D, M-mode echocardiographic measurements were done. Past studies have reported possible effects of tamoxifen and Cre expression alone on heart function. Koitabashi et al. (2009) report a dilated cardiomyopathy and reduced heart function in αMHC-MCM mice once injected with 80 mg/kg tamoxifen for 5 days. Similarly, Hall and team (2011) observed reduced fractional shortening in αMHC-MCM mice following injection of 40 mg/kg tamoxifen for 5 days. These alterations were not observed in mice receiving 1 or 3 injections of tamoxifen (Hall et al. 2011). Hougen et al. (2010) have previously demonstrated that 4 tamoxifen injections (40 mg/kg) can cause a similar reduction in heart function as reported by Hall and team (2011). Buerger et al. (2006) also reported dilated cardiomyopathy in hearts expressing Cre-recombinase alone in the absence of tamoxifen treatment. Lifespan was also reduced to 11-13 weeks in these mice; normal average lifespan of laboratory mice is approximately 24 months. Initial measurements were performed to rule out possible direct effects of tamoxifen and MCM on the measured myocardial parameters in my study. αMHC-MCM/STX1A flox/flox mice were injected with peanut oil (control) and were compared to wild-type mice injected with tamoxifen (TAM; n=3) and Cre positive mice injected with tamoxifen (Cre+; n=5). The latter two groups were given four lower doses of tamoxifen injections (20 mg/kg) over a 4-day period. All 3 groups showed no baseline differences prior to the tamoxifen treatment (time -1 week) in systolic dimension, systolic volume, diastolic dimension, diastolic volume, heart rate, stroke volume, software-generated cardiac output, and calculated cardiac output (Figures 4 and 5).

Baseline systolic dimension (Ds) for control mice were 2.29 ± 0.06 mm, TAM: 2.48 ± 0.24mm, and Cre+: 2.22 ± 0.22mm (Figure 11A). These values agree with those reported in literature of 2.18 ± 0.3 mm (Sohal et al. 2001) and 2.1 ± 0.3 mm (Colazzo et al. 2015). Diastolic dimension (Dd) for all 3 groups (Control: 3.71 ± 0.08 mm, TAM: 3.85 ± 0.22 mm, Cre+: 3.47 ± 0.23 mm) agree with previously observed values of 3.78 ± 0.27 mm (Figure 11C) (Sohal et al. 2001) and 3.7 ± 0.3 mm (Colazzo et al. 2015). Systolic volume (Vs) shown in Figure 11B for control (18.3 ± 1.2 μL), TAM (23.1 ± 4.9 μL), and Cre+ (17.8 ± 4.6 μL) concur with the 13.8 ± 4 μL SV in C57BL/6 mice reported by Colazzo et al. (2015) and 17.5 ± 4.63 μL by Chu et al. (2015). Colazzo and team (2015) reported a diastolic volume (Vd) of 53 ± 8 μL which overlaps with ranges in this thesis (Control: 59.1 ± 3.0 μL, TAM: 67.3 ± 7.9 μL, Cre+: 51.2 ± 7.9 μL; Figure 11D). These values also agree with the Vd 77.50 ± 17.53μL observed by Chu et al. (2015).

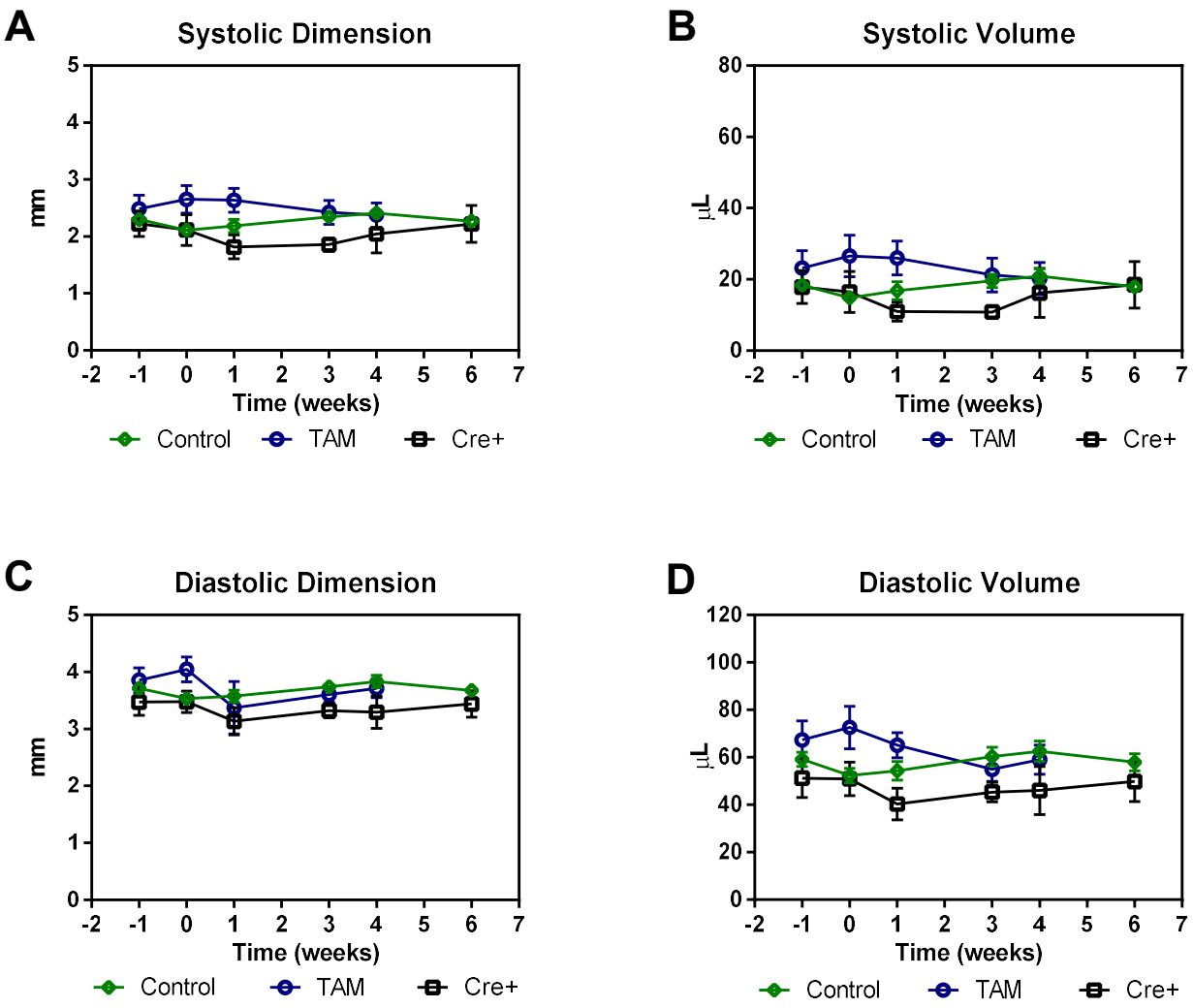

Figure 11: Effects of tamoxifen and Cre on systolic and diastolic dimensions and volumes. Transthoracic 2D M-mode echocardiographic measurements were performed to assess systolic and diastolic dimensions and volumes, over a 6-week period. Systolic dimension (A), systolic volume (B), diastolic dimension (C), and diastolic volume (D) of control mice (green diamonds; n=11), WT mice treated with tamoxifen (TAM, blue circles; n=3), and Cre expressing mice (Cre+, black squares; n=5) are displayed. Data points are the means ± SEM. All data were collected and analyzed using VisualSonics Vevo 2011 high resolution ultrasound imaging system. A one-way ANOVA followed by a Tukey test was used to determine significance at each time point (p <0.05). No statistical differences were observed.

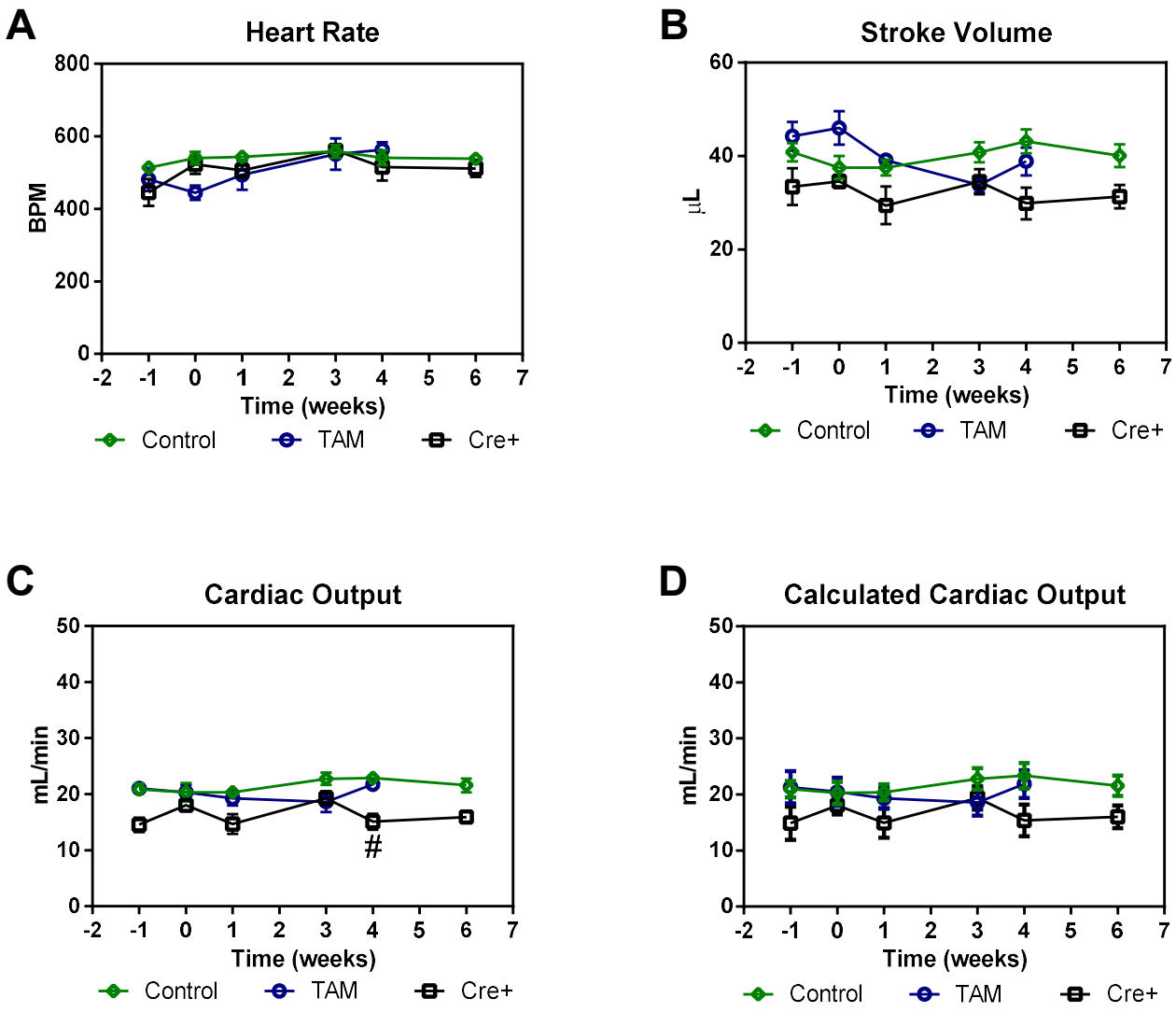

Figure 12: Effects of tamoxifen and Cre expression on heart rate (A), stroke volume (B), cardiac output (C) and calculated cardiac output (D). Control mice (green diamonds; n=11), WT mice treated with tamoxifen (TAM, blue circles; n=3), and Cre expressing mice (Cre+, black squares; n=5) are shown. Cardiac output data denote values obtained from the software while the calculated cardiac out was determined from the individual product of heart rate and stroke volume. All data were collected and analyzed using VisualSonics Vevo 2011 high resolution ultrasound imaging system. Values shown are mean±SEM. A one-way ANOVA followed by a Tukey test was used to determine significance at each time point (p <0.05). '#' represents statistical difference between control and Cre+ groups.

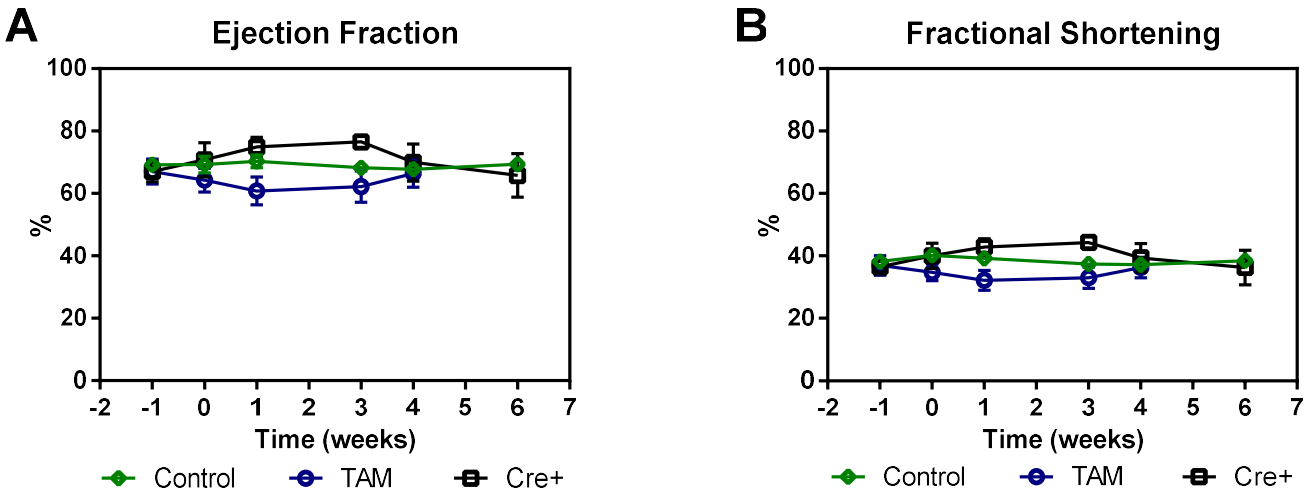

Figure 13: Effects of tamoxifen and Cre on ejection fraction and fractional shortening. Ejection fraction (A) and fractional shortening (B) of control mice (green diamonds; n=11), WT mice treated with tamoxifen (TAM, blue circles; n=3), and Cre expressing mice (Cre+, black squares; n=5) are displayed. All data are the means ± SEM and were collected and analyzed using VisualSonics Vevo 2011 high resolution ultrasound imaging system. A one-way ANOVA followed by a Tukey test was used to determine significance at each time point (p <0.05).

The baseline HR (Figure 12A; beats per min - BPM) for control (513 ± 12 BPM), TAM (481 ± 31 BPM), and Cre+ (445 ± 36 BPM) were not significantly different from each other and agree with previously reported values in male C57BL/6 mice ranging from 438 (Janssen et al. 2004) to 530 BPM (Colazzo et al.2015; Chu et al. 2015; Yang et al. 2017). As determined by Colazzo et al. (2015), the stroke volume (SV) of C57BL/6 male mice falls within 39 μL. Pleasant-Jenkins et al. (2017) reported SV in C57BL/6 mice between and 30-35 μL. The baseline SV for control (40.8 ± 1.9 μL), TAM (44.2 ± 3.0 μL), and Cre+ mice (33.4 ± 3.9 μL) lay within these published ranges (Figure 12B). In the same publications, cardiac output (CO) was reported at 19.8 ± 4 mL/min. This agrees with both the software-generated CO (Figure 12C) and calculated CO (Figure 12D) –CO; Control: 20.8 ± 1.0 mL/min, TAM: 21 ± 0.3 mL/min, Cre+: 14.5 ± 1.26 mL/min. Calculated CO; Control: 20.9 ± 1.5 mL/min, TAM: 21.3 ± 2.9 mL/min, Cre+: 14.9 ± 2.9 mL/min.

Values for ejection fraction (EF) have varied in the literature ranging from 65-66% (Popovic et al.2005; Yang et al. 2017) to 74-77% (Colazzo et al. 2015; Chu et al. 2015). Baseline EF (Control: 69 ± 1%, TAM: 67 ± 7%, Cre+: 67 ± 3%) in my experiments fall within these ranges (Figure 13A). FS baselines (Figure 13B) for Control: 38.2 ± 0.8%, TAM: 36.9 ±3.1% and Cre+: 36.5 ± 2.3% agree with observations by Gao et al. (2011) and Chu et al. (2015) of 40 ± 2% and Colazza et al. (2015) of 44 ± 6%.

In summary, injections of peanut oil in αMHC-MCM/STX1A flox/flox mice and tamoxifen for TAM and Cre+ mice, Ds, Dd, Vs, Vd, HR, SV, calculated CO, EF, and FS remained unchanged over the 6-week monitoring period (Figures 11, 12 and 13) with the

exception of the software-generated CO (Figure 12C). The Cre+ software-generated CO was significantly different at 4 weeks following the final tamoxifen injection when compared to the control and TAM groups. This difference, however, is not carried over to the calculated CO (Figure 12D). Overall, my results failed to show any direct effect of tamoxifen or Cre expression on heart function as has been reported previously.

3.4 Heart Function of STX1A KO Mice

To investigate the effects of STX1A deficiency on heart function, cardiac-specific STX1A KO mice (n=12), referred to as STX1A KO from here on in, were compared to Cre+ mice. All baseline values for αMHC-MCM/STX1A flox/flox mice prior to tamoxifen treatment agreed with the published values for the functional parameters mentioned above. A day after the 4^{th} injection of tamoxifen (0 Week Post), there was marked reductions in myocardial function as observed by the 2D M-mode echocardiographic measurements (Figure 14).

Significant increases in Ds and Vs were seen in the STX1A KO group (week 0; $p<0.05$). This increase was found to persist from 0-3 weeks post tamoxifen injection with the greatest spike at 0 weeks and recovery by 4 weeks (Figure 15A and 15B). Ds increased to 3.37 ± 0.25 mm from a baseline of 2.27 ± 0.07 mm at 0 weeks. Ds gradually declined to 2.76 ± 0.23 mm at 1 week and 2.58 ± 0.11 mm at 3 weeks post-tamoxifen treatment. By week 4 post-tamoxifen treatment, Ds returned to similar levels as the Cre+ group (2.53 ± 0.11 mm). Vs for STX1A KO (Figure 15B) followed a similar trend with an initial spike from 18.05 ± 1.48 µL to 51.73 ± 8.86 µL (0 week) followed by decreases to 32.11 ± 7.19 µL (1 week) and then 25.20 ± 3.03 µL (3 weeks). By the 4^{th} week, Vs returned to 24.05 ± 2.69 µL which was not significantly

different from the Cre+ mice. This trend is seen in the representative traces which show reduced LV wall movement during systole 0-week post-TAM with partial recovery by 3 weeks (Figure 14). Similarly, Vd was found to increase in STX1A KO mice at 0- and 3-weeks post tamoxifen with recovery by 4 weeks (Figure 15C). Vd increased from a 56.55 ± 3.2 μL baseline to 81.38 ± 7.11 μL by week 0. Vd at 1 week (63.41 ± 6.38 μL) was not significantly different from Cre+ mice; however, at 3 weeks post-tamoxifen treatment, 62.36 ± 4.38 μL was significantly greater relative to the Cre+ group. By 4 weeks post-tamoxifen treatment, Vd had decreased to 58.65 ± 3.63 μL which were not statistically different from Cre+ mice. Dd was only statistically greater at 3 weeks post-tamoxifen treatment with a dimension of 3.78 ± 0.11 mm.

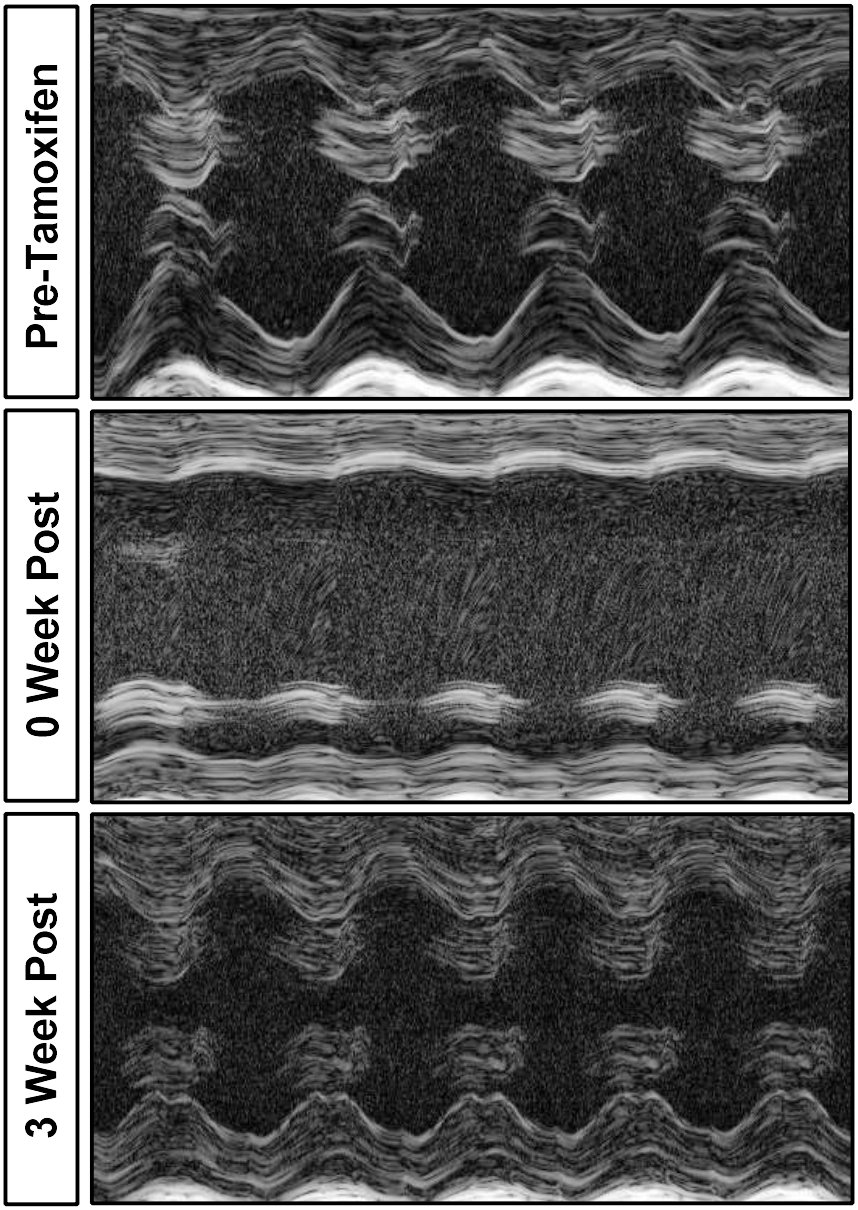

Figure 14: Representative transthoracic 2D M-mode echocardiographic images. Images for pre-tamoxifen injected mice and mice injected with tamoxifen at 0-week post tamoxifen (immediately following the 4-day injections), and 3-week post-tamoxifen injection are shown. Images were taken on anesthetized mice using VisualSonics Vevo 2011 high resolution ultrasound imaging system (cardiology package).

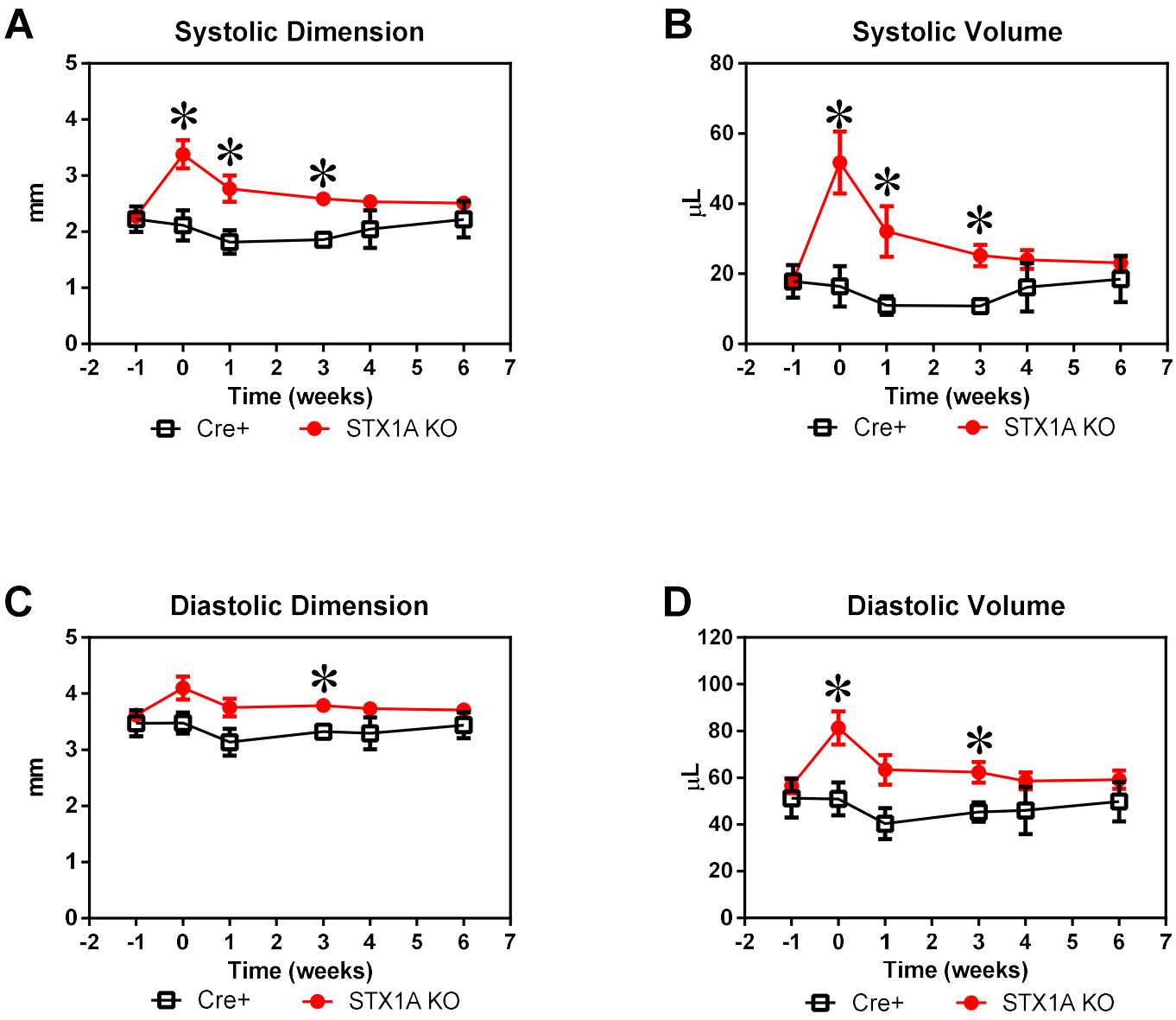

Figure 15: The effects of STX1A deletion on myocardial systolic and diastolic function. Systolic dimension (A), systolic volume (B) diastolic dimension (C), and diastolic volume (D) of STX1A knockout (KO) mice (red filled circles; n=12) and Cre+ (black; n=5) are displayed. The x-axis represents number of weeks with -1 being the pre-injection values. Data points represent the means ± SEM and were collected and analyzed using VisualSonics Vevo 2011 high resolution ultrasound imaging system (M-mode). A one-way ANOVA followed by a Tukey test was used to determine significance at each time point (p <0.05). Points of significant difference are indicated by an asterisk.

The mean HR, SV, and calculated CO were not different over the 6 weeks (Figure 16A, B and D), whereas the software-generated CO showed baseline differences in CO (-1 week) between the STX1A KO group and Cre+ group prior to tamoxifen injections (Figure 16C). Following the final tamoxifen injection, this difference was no longer observed with the exception at 4 weeks post tamoxifen. EF and FS were also found to decrease over the 0-3 weeks post tamoxifen period in STX1A KO mice (Figure 17). It was noted the greatest decrease in EF and FS was at week 0 which by week 4 returned to similar levels as Cre+ mice. For EF, a reduction from a baseline of 68.1 ± 1.5% to 41.6 ± 5.6% at week 0 was seen. This was followed by an increase in EF to 54.5 ± 5.4% at week 1 and to 60.6 ± 1.8% at week 3. By week 4, EF had increased to 61.1 ± 2.3% and was not significantly different from Cre+ mice. FS, mirroring EF, displayed an initial drop from a baseline of 37.5 ± 1.2% to 21.1 ± 3.2% at week 0 followed by an increase to 28.8 ± 3.3% by week 1. By week 3, FS had increased to 31.9 ± 1.3% and by week 4 with a FS of 32.4 ± 1.6%, was not significantly different from the Cre+ group.

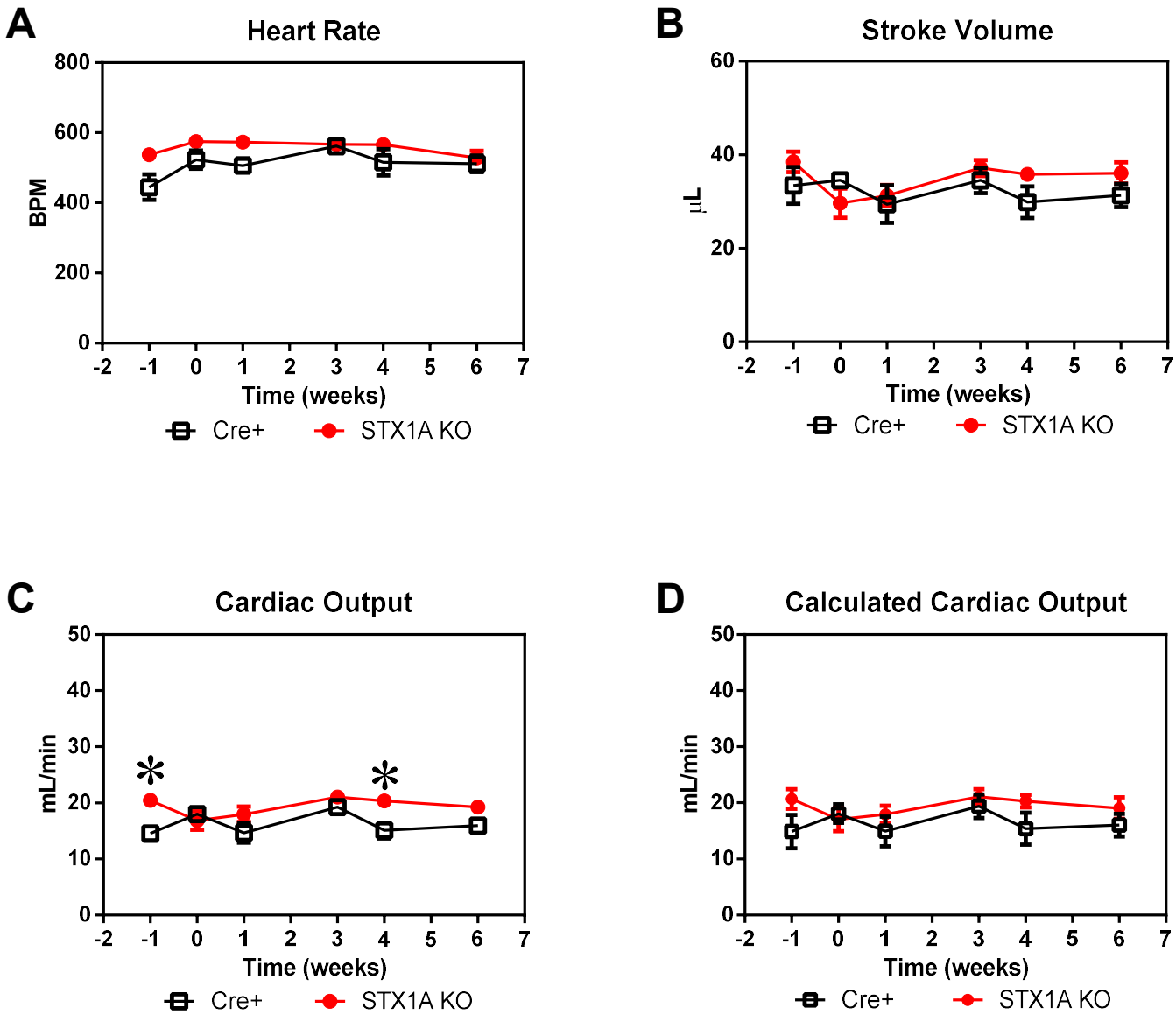

Figure 16: The effects of STX1A deletion on heart rate, stroke volume and cardiac output. Heart rate (A), stroke volume (B), cardiac output (C), and calculated cardiac output (D) of STX1A KO mice (red filled circles; n=12) and Cre+ mice (black open squares; n=5) are shown. Cardiac output data denote values obtained from the software while the calculated cardiac output was determined from the individual product of heart rate and stroke volume. Data points are the means ± SEM. A one-way ANOVA followed by a Tukey test was used to determine significance at each time point. Statistical significance is indicated by an asterisk (p <0.05).

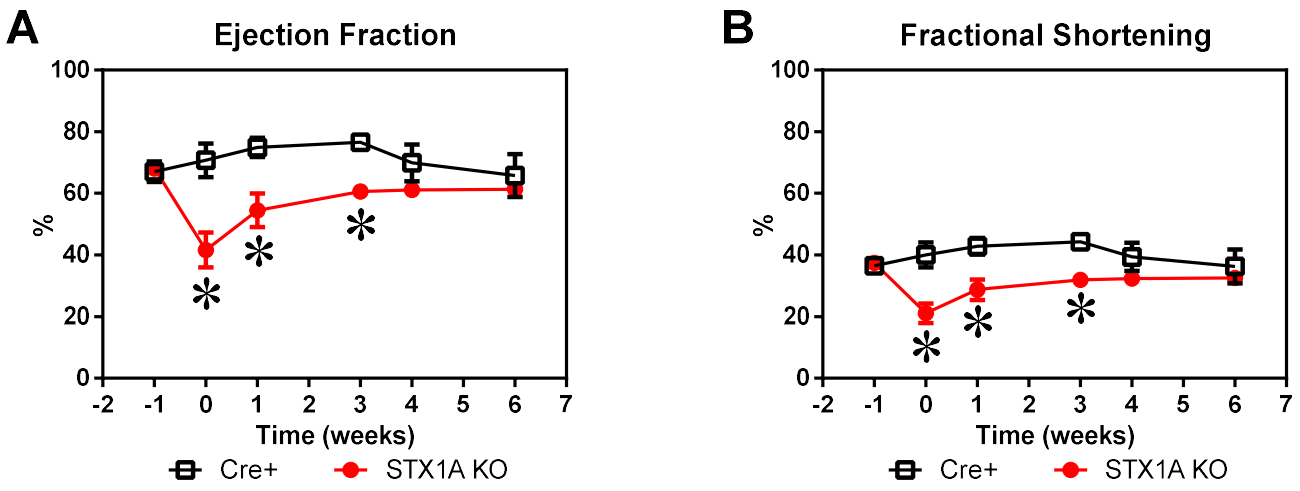

Figure 17: The effects of STX1A deletion on ejection fraction and fractional shortening. Ejection fraction (A) and fractional shortening (B) for STX1A KO mice (red circles; n=12) and Cre+ mice (black squares; n=5) are displayed. A one-way ANOVA followed by a Tukey test was used to determine significance at each time point. Statistical difference is indicated by an asterisk (p <0.05).

3.5 Invasive Hemodynamics Assessing Left Ventricle Pressure Generation

Echocardiography data show reduced systolic function in STX1A KO mice. To further assess whether this declined function is a result of reduced contractility of the left ventricle or an indirect result of elevated afterload, hemodynamic measurements were done. Using a solid-state catheter, LV pressure (LVP), peak rate of pressure change (dP/dt), aortic pressure (AoP) and HR were measured prior to tamoxifen injections (-1 week), after the tamoxifen treatment (week 0), and 3 weeks post-tamoxifen treatment (Figure 18). LVP and AoP during systole and diastole were found to remain unchanged after the administration of tamoxifen to αMHC-MCM/STX1A flox/flox mice (Figure 18 A and 18B). Baseline systolic LVP (LVPs) prior to tamoxifen treatment was 95.6 ± 2.8 mmHg (Figure 18A). Following the tamoxifen treatment (week 0) LVP of STX1A KO mice was 86.9 ± 7.3 mmHg and 3 weeks post-tamoxifen treatment was 97.6 ± 1.9 mmHg. These values agree with previous studies which have reported baseline LVPs ranging from 80 to 119 mmHg (Fan et al. 2013; Jacoby et al. 2006; De Waard et al. 2007). Baseline diastolic LVP (LVPd) was determined to be 2.9 ± 2.1 mmHg (Figure 18A). At week 0, these mice had a LVPd of 6.7 ± 1.3 mmHg and at week 3 of 4.8 ± 1.2 mmHg. These values for LVPd agree with those previously published as they fall in the range of 2.0-6.5 mmHg (Fan et al. 2013; Jacoby et al. 2006; De Waard et al. 2007). Systolic AoP (sAoP) before tamoxifen treatment was 91.1 ± 4.3 mmHg (Figure 18B). Following the tamoxifen treatment, sAoP was not significantly altered in STX1A KO mice. sAoP was 98.0 ± 5.7 mmHg at 0 week and at 3-week post-tamoxifen treatment was 93.8 ± 1.3 mmHg. These values agree with sAoP values previously reported of 99 ±3 mmHg by Izumiya et al. (2006) and Kelsey et al. (2013). sAoP of 98.5 ± 2.9 and 96.8 ± 2.5 mmHg have also been reported by Muthuramu and team (2013 and 2017). Similarly, no change in diastolic AoP (dAoP) was seen in STX1A KO mice (66.2 ± 4.0 mmHg, -

1 week; 69.6 ± 3.5 mmHg, 0 week; 69.4 ±1.1 mmHg, 3 weeks; Figure 18B).These values agree with previously published dAoP pressures ranging between 62 to 73 mmHg (Muthuramu et al. 2013, 2017) and 70 to 80 mmHg (Kelsey et al. 2013).

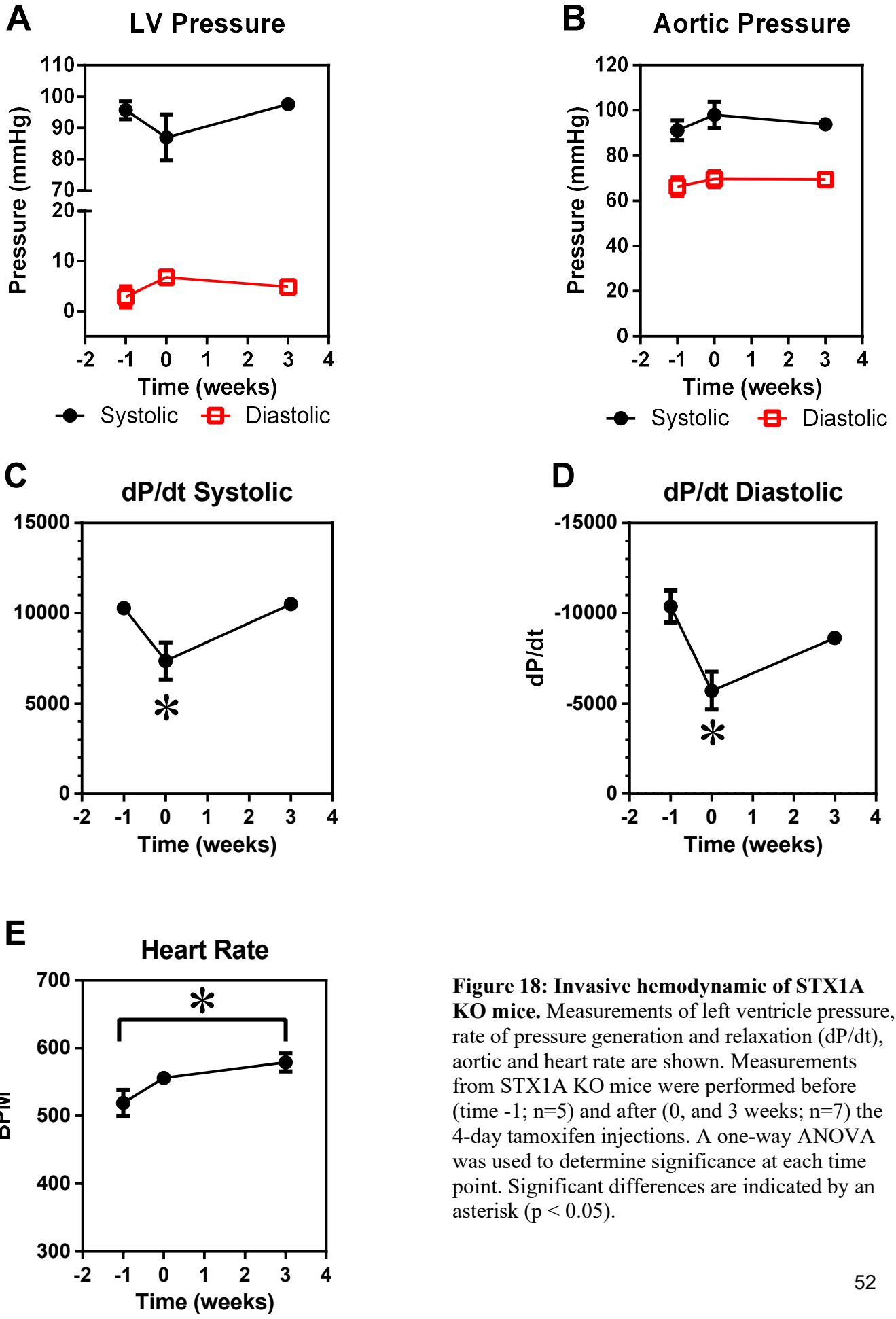

Figure 18: Invasive hemodynamic of STX1A KO mice. Measurements of left ventricle pressure, rate of pressure generation and relaxation (dP/dt), aortic and heart rate are shown. Measurements from STX1A KO mice were performed before (time -1; n=5) and after (0, and 3 weeks; n=7) the 4-day tamoxifen injections. A one-way ANOVA was used to determine significance at each time point. Significant differences are indicated by an asterisk ($p < 0.05$).

Systolic dP/dt (also referred to as dP/dt max) at week1 was 10,279 ± 205 mmHg/s (Figure 18C). At week 0 mice displayed a reduced rate of 7354 ± 1009 mmHg/s. By week 3, systolic dP/dt had increased to 10,502 ± 356 mmHg/s; levels comparable to the baseline. Following a similar trend, baseline diastolic dP/dt (also referred to as dP/dt min) was -10,363 ±879 mmHg/s. At week 0, diastolic dP/dt was reduced to -5702 ± 1040 mmHg/s and by week 3 had increased to -8635 ± 310 mmHg/s which is not significantly different from the baseline. The absolute values observed for baseline and 3 weeks post tamoxifen treatment systolic and diastolic dP/dt do fall higher than those more commonly reported in literature ranging between 5000-8000 mmHg/s (De Waard et al. 2007; Fan et al. 2013; Fukushima et al. 2011). However, values above this range are not novel as Jacoby and team (2006) reported dP/dt max of 10,001 ± 3144 mmHg/s. Rates as high as 22,254 ± 1,035 mmHg/s have also been reported (Joho et al. 2006; Yang et al. 2017).

HR measured during invasive hemodynamics was found to increase in STX1A KO mice by week 3; however; this was not observed during echocardiography. Prior to the tamoxifen treatment, HR was measured to be 519 ± 19.2 BPM which agrees with baseline HR values measured via echocardiography in this thesis and past publications as mentioned previously (Colazzo et al.2015; Chu et al. 2015; Yang et al. 2017). Baseline HR of 563 ± 75 and 537 ± 8 BPM have been observed in hemodynamic experiments by Jacoby et al. (2006) and De Warrd et al (2007), respectively. At week 0, HR was 556 ± 9.6 BPM and at week 3 HR was measured at 579 ± 13.2 BPM. Overall, hemodynamic data failed to show any change in LVPs/d and s/dAoP in STX1A KO mice but showed a decrease in peak systolic and diastolic dP/dt at week 0 with increased HR at week 3.

3.6 Delay between R-wave and Onset of Contraction

During my measuring of the echocardiographic parameters I noticed an apparent delay between the start of the R wave of the ECG to the onset of contraction. I decided to quantify the time delay between the R-wave peak and the onset of LV posterior wall contraction. Control, Cre+, and STX1A KO mice showed no difference prior to their respective treatments of peanut oil or tamoxifen (Pre-injection Control: 8.7 ± 1.3 msec; Cre+: 8.3 ±1.1 msec; STX1A KO: 8.8 ± 0.9 msec; Figure 19). Control mice over the 6-week period remained at baseline levels (0 week: 8.7 ± 0.8 msec; 1 week: 9.1 ± 1.5 msec; 3 weeks: 9.4 ± 1.3 msec; 4 weeks: 7.9 ± 0.8 msec; 6 weeks: 9.8 ± 1.3 msec). Cre+ mice were not significantly different than the control with the exception of week 4 post-tamoxifen treatment. At 4 weeks, Cre+ mice showed an increased delay of 12.5 ± 1.7 msec whereas the control mice were at 7.9 ± 0.8 msec. This was not seen at week 6. Cre+ mice; 0 week: 11.9 ± 1.9 msec; 1 week:13.6 ± 2.5 msec; 3 week: 9.3 ± 1.9 msec; 4 week: 12.5 ± 1.7 msec; 6 week: 11.1 ± 0.7msec. STX1A KO mice remained at comparable levels to Cre+ mice throughout the 6 week monitoring period but were significantly higher than the control group with the exception of week 3 (STX1A KO mice; 0 week: 16.2 ± 1.8 msec; 1 week:18.7 ± 1.5 msec; 3 week: 11.3 ± 1.0 msec; 4 week: 12.9 ± 1.1 msec; 6 week: 13.8 ± 1.0 msec). Overall, control mice displayed no change in delay between R-wave and onset of contraction whereas, STX1A KO mice show a greater transient spike in delay at week 0 and 1 but by week 4 and 6 have reduced times which are still greater than those observed in control mice. Cre+ mice mirrored the STX1A KO mice trend at a lower magnitude.

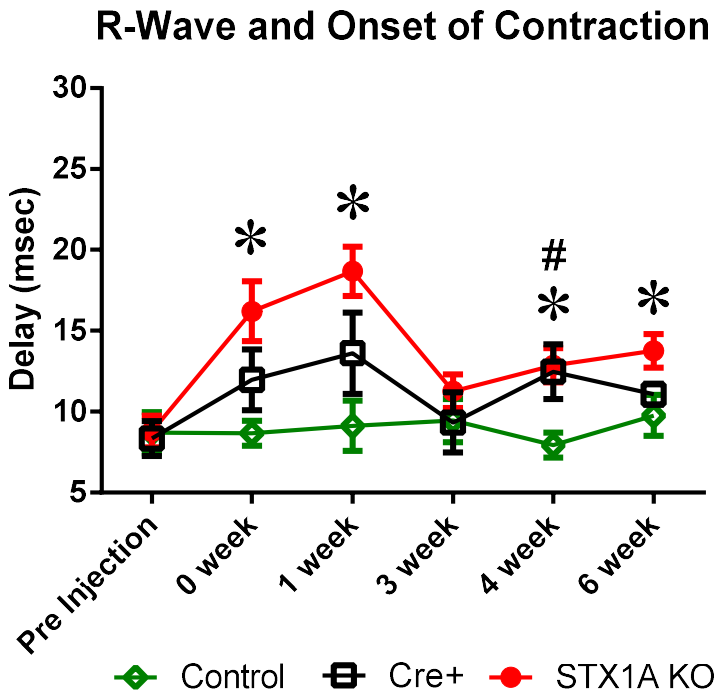

Figure 19: The delay between R-wave and onset of contraction in STX1A KO mice. The time between the R wave on the onset of contraction was measured from control mice (green diamonds; n=11), Cre+ mice (black squares; n=5), and STX1A KO mice (red circles; n=12). All data were collected and analyzed using VisualSonics Vevo 2011 high resolution ultrasound imaging system. A one-way ANOVA followed by a Tukey test was used to determine significance. An asterisk indicates a significant difference between the control and STX1A KO mice. '#' indicates a significant difference between control and Cre+ mice. No significant difference was observed between the Cre+ and STX1A KO mice.

3.7 Myocardial Hypertrophy in STX1A KO Mice

Compensatory cardiac hypertrophy has been shown to be a common response to heart failure (Anversa et al. 1991; Izumiya et al. 2006). Using echocardiography, LV posterior wall thickness was measured to assess possible hypertrophy in STX1A KO mice. No change in wall thickness was seen over the 6 weeks within or among the groups (Figure 20A). A baseline posterior wall thickness for Control, TAM, Cre+, and STX1A KO mice lay between 0.86 – 1.08 mm and at 6 weeks post-treatment this range was 0.93 – 1.06 mm. These values agree with published diastolic LV posterior wall thickness measurements which range from 0.69 to 0.97 mm (Colazzo et la. 2015; Ma et al. 2012).The same trend was shown for heart weight-to-tibia length ratios (Figure 20B) as observed in αMHC-MCM/STX1A flox/flox mice prior to tamoxifen treatment (Pre), 0 week post-treatment, and 3 week post-treatment were not statistically different - Pre: 7.2 ±0.5 g/cm, 0 week: 6.4 ± 0.2 g/cm, 3 weeks: 6.9 ± 0.5 g/cm. These ratios agree with those reported in literature by Pallai et al. 2006 (6-7 mg/mm), Trivedi et al. 2008 (7.0 ± 1.5 mg/mm), and Zheng et al. 2010 (6.4 ± 1.8 mg/mm). Overall, my results do not show evidence of hypertrophy in STX1A KO mice.

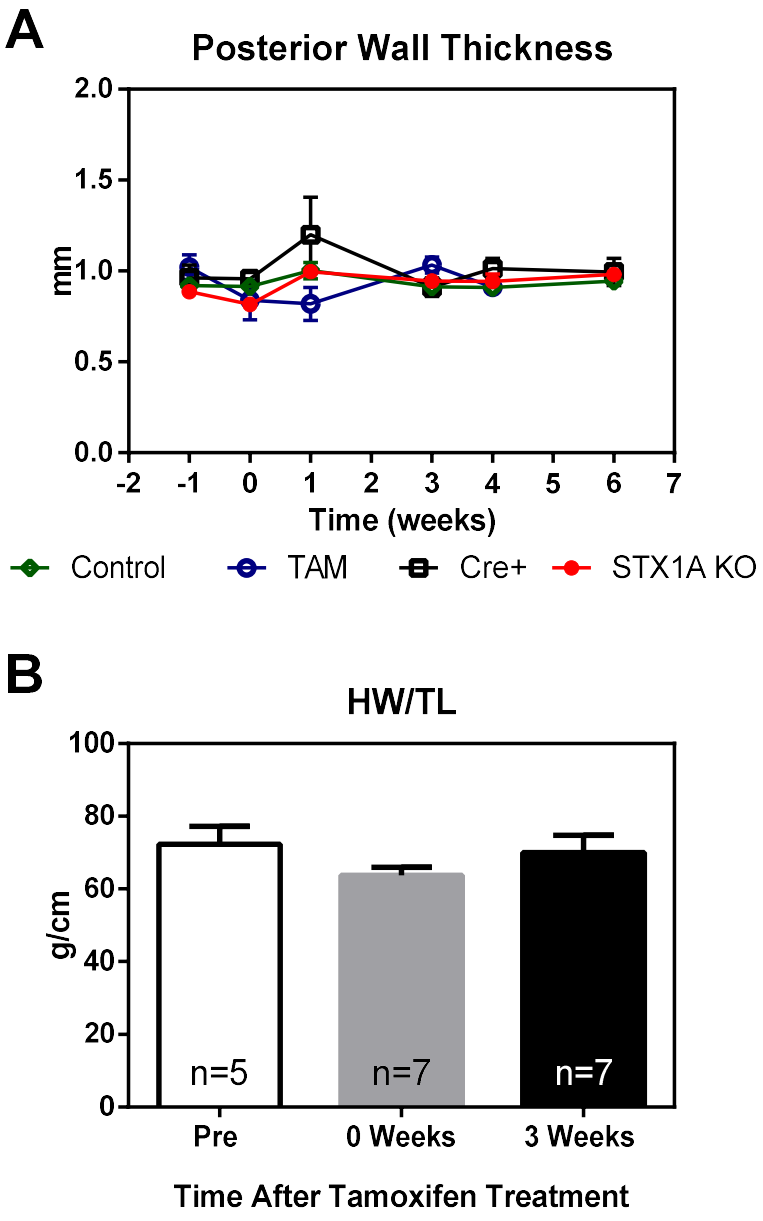

Figure 20: Assessment of myocardial hypertrophy. The posterior wall thickness (A) over the 6-week period for control mice (green diamonds; n=11), WT treated with tamoxifen (TAM, blue open circles; n=3), Cre positive mice (Cre+, black squares; n=5) and STX1A KO mice (red filled circles; n=12). Heart weight to tibia length ratios (B) of male STX1A flox/flox mice before (n=5), 0 weeks post (n=7), and 3-week (n=7) post-tamoxifen injections. A one-way ANOVA was used to determine significance. No statistical differences were observed.

3.8 Possible Compensation by other SNARE Proteins

In echocardiography and invasive hemodynamic data presented above, STX1A KO mice demonstrated recovery by 3 weeks post tamoxifen treatment. Western blots were used to access for possible compensatory increase in expression of other SNARE proteins similar in function to STX1A in the heart. These SNAREs consisted of STX2, 3, and 4 (Ferlito et al. 2010, Mandon et al. 2017). Western blots for STX 2 and 3 (not shown) were inconsistent and unsuccessful in detecting the protein of interest. Western blot for STX4 showed the predicted bands of 34 kDa in the skeletal muscle (SM; positive control) as well the control and STX1A KO LVs and IVSs (Figure 21A). Densitometry analysis for STX4 shows a possible increase in STX4 levels in STX1A KO mice (Figure 21B. The blot was done once (n=2) so the trend remains to be confirmed.

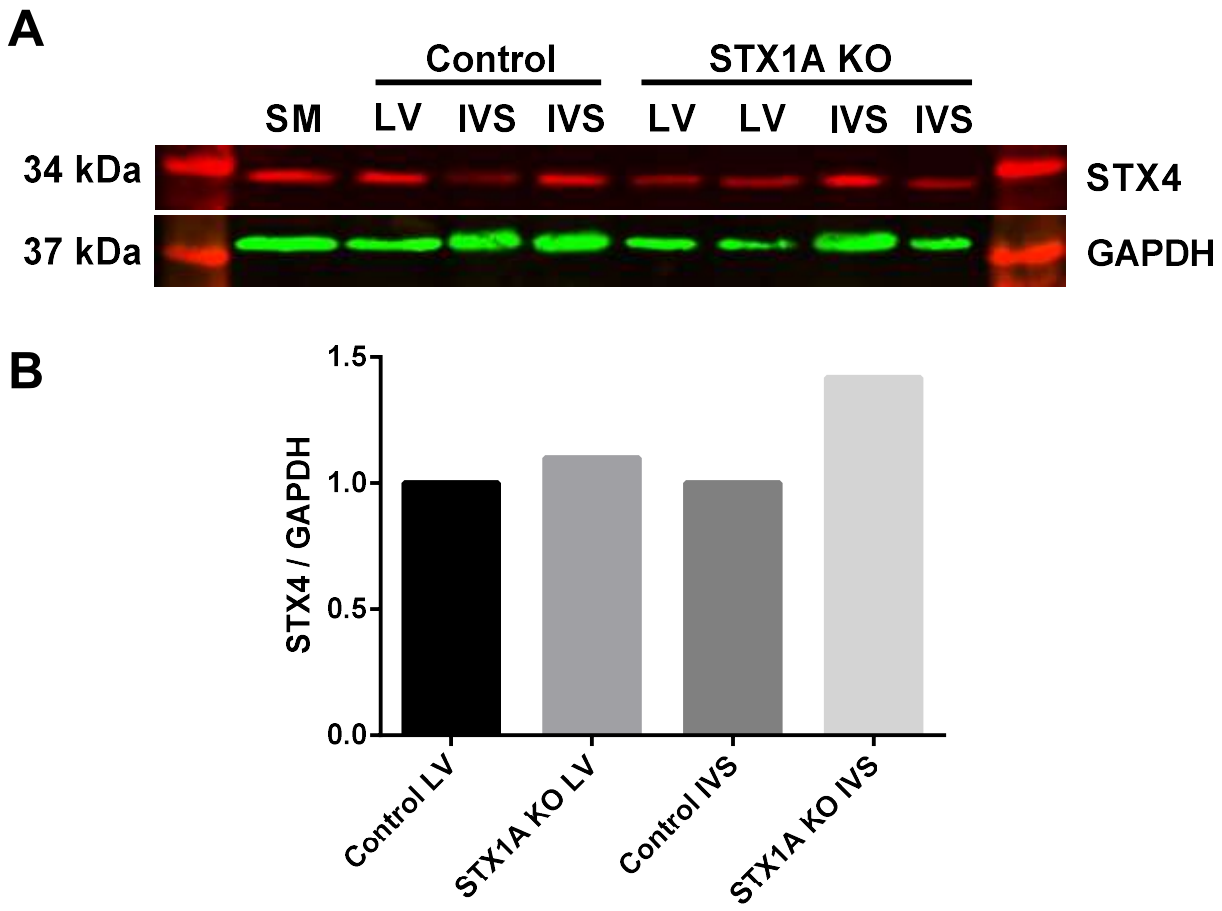

Figure 21: Western blot analysis of syntaxin 4 (STX4) from isolated LV and interventricular septa (IVS). Protein lysates from αMHC-MCM STX1A floxed mice injection with peanut oil (control) and those which were tamoxifen treated (STX1A KO) were resolved by SDS-PAGE. Each well contained 30 µg of protein. Skeletal muscle (10 µg) served as a positive control for STX4. Rabbit polyclonal antibody for syntaxin 4 (1:1000) was used. A positive result was observed at ~34kDa. Membrane were visualized using a LI-COR Odyssey infrared imaging system (n=1).

Chapter Four: Discussion

4.1 Summary of Results

Since the discovery of SNARE proteins, a lot has been uncovered about the vital roles this protein super family plays throughout the body with a major emphasis on the brain (Jahn and Scheller 2006). These proteins have also been studied in other organs such as the heart (Peters et al. 2006). Relatively speaking, much less is known about their roles in cardiac muscle especially that of STX1A. The aim of this thesis was to help shed light on the function of STX1A in the heart. It was initially, hypothesized that STX1A knockout hearts will display increased inotropy and chronotropy. The basis of this hypothesis was that once STX1A was removed, voltage-gated calcium channels in the heart will no longer be inhibited by STX1A (Arien et al. 2003; Wiser et al. 1996, 2002). This would allow for increased rate and amplitude of calcium transients resulting in stronger and faster contractions (Bers 2002; Fabiato 1983). The observations from this thesis are contradictory to this initial prediction. To test this hypothesis, cardiac-specific-STX1A knockout C57BL/6 mice were used. PCR genotyping confirmed the presence of αMHC-MCM and STX1A flanking loxP sites in these mice. Following tamoxifen treatment, STX1A KO was confirmed through immunohistochemistry. Echocardiography measurements showed no differences in Ds, Vs, Dd, Vd, HR, SV, EF, FS, and calculated CO in Control, TAM, and Cre+ groups. In STX1A KO mice however, Ds and Vs were significantly elevated over the 0-3 week post tamoxifen treatment period. EF and FS in STX1A KO mice were significantly reduced over this same time frame. These patterns are suggestive of systolic dysfunction in STX1A KO heart. HR, SV, and calculated CO were observed to be unaffected as a result of STX1A KO. Invasive hemodynamics demonstrated no change in LVPs/d and AoPs/d in response to STX1A KO. However, systolic and diastolic dP/dt were seen to be reduced at week 0 which recovered by 3-

week post-tamoxifen treatment. Both posterior wall measurements and HW/TL ratios demonstrated no hypertrophy in response to STX1A KO hearts. Interestingly, a delay between the R-wave and onset of LV contraction was noted in STX1A KO mice relative to Control mice, but not when compared to Cre+ mice.

4.2 Confirmation of STX1A Knockout Using Immunohistochemistry

Despite screening each mouse for the required homozygotic LoxP sites flanking exons 2 and 3 of *STX1A* and the αMHC-MCM construct, western blots on tamoxifen treated hearts were unable to confirm STX1A KO. However, the expression of Cre recombinase in these hearts was confirmed using western blots. Further, the possibility of STX1A contamination from nerve terminals during heart isolation was also ruled out because SYN1, a neuronal marker, was not detected by western blots on LV or IVS (De Camilli et al 1983; Mishima et al. 2014). Various anti-bodies against STX1A from either a rabbit or mouse host were used in efforts to confidently detect a STX1A band in control hearts with its absence or reduction in tamoxifen treated hearts. The results obtained from these series of western blots appeared highly variable and were unable to indicate successful knockout or knockdown. The inability to detect STX1A using traditional western blot methods can be speculated and attributed to the following. One of the more common reasons of western blot variability can be traced back to the primary anti-bodies (Ghosh et al. 2014). It is not uncommon that primary anti-bodies in laboratory setting fail to detect their intended antigens when used in different tissues and/or cell types. This was particularly seen in western blots that contained both brain and heart samples. The lanes that contained LV lysates displayed a much greater number of bands than in the brain (positive control), indicative of

greater non-specific binding by the same primary anti-body in heart lysates. Considering the underlining principle of western blots, to separate proteins by molecular weight in their primary denatured states, could hinder efficiency and/or affinity of primary antibodies in detecting their intended antigens (Ghosh et al. 2014). It has also been observed that the centrifugation and removal of cellular debris could cause great loss of target protein, interfering with protein detection or quantification (Ghosh et al. 2014; Murphy et al. 2009). It was found that the removed cellular debris when preparing rat skeletal muscle lysates contained a significant proportion of myosin and calsequestrin-2 (Murphy et al. 2009). This could very well cause inaccuracies when using western blots as a quantitative measure in determining changes in protein expression levels. A simple way to avoid this issue is to load a more diluted but crude lysate (Ghosh et al. 2014). Finally, activity of endogenous proteases may also produce inconsistencies among samples. Even with the use of protease inhibitors, it is recommended that samples be frozen in liquid nitrogen as quickly as possible for storage to minimize protein degradation. The samples used in this thesis were stored on dry ice during collection and transferred to a -80^{o}C freezer for storage. In efforts to circumvent these potential challenges, immunohistochemistry was used as well. Ramos-Vara (2005) describes formaldehyde as the gold standard when it comes to immunohistochemistry fixation. Through paraformaldehyde fixation of heart samples followed by antigen retrieval, protein preservation was maximized. In addition, primary antibodies are allowed to interact with their target proteins in their higher order native structures, as denaturization is not necessary. With this method the predicted location of the target protein can also be used in assessing signal accuracy as certain proteins, such as STX1A are localized to the sarcolemma (Brose 2014). Immunohistochemistry was able to successful demonstrate STX1A KO in the LV by 0- and 3-weeks post tamoxifen treatment.

4.3 Cardiotoxic Effects of Tamoxifen and/or Cre on Heart Function

The tamoxifen inducible Cre-loxP system has become a popular choice for tissue-specific and temporal-specific manipulation of gene expression (Koitabashi et al. 2009). However, past studies have demonstrated that the use of such a technique in cardiac tissue can potentially produce cardiotoxicity, which in turn reduces systolic function (Koitabashi et al. 2009). These effects have been attributed to either the presence of tamoxifen, Cre, or both. As discussed previously, Koitabashi et al. (2009) observed dilated cardiac myopathy and reduced systolic function in response to five 80mg/kg tamoxifen injections administered to C57BL/6 mice carrying the αMHC-MCM construct but not Cre negative mice. It was also seen that half of this dosage (40mg/kg) was also able to reproduce these effects in mice after 5 injections but not when given 1 or 3 injections (Hall et al. 2011). Hougen et al. (2009), following a similar injection protocol to Hall and team (2011), observed reduced heart function in response to four injections of 40 mg/kg of tamoxifen. These results were explained by global changes in gene expression of proteins vital for excitation-contraction coupling in cardiomyocytes. The presence of Cre, independent of tamoxifen, has also been argued to produce the aforementioned effects (Buerger et al. 2006).

In this thesis a concentration of 20 mg/kg of tamoxifen was used to induce MCM, which is half of the lowest concentration shown to effect heart function in mice. No evidence of tamoxifen or Cre induced cardiotoxicity was seen in this thesis. Control mice (injected with peanut oil only), TAM mice (wild-type mice injected with tamoxifen), and Cre+ mice (αMHC-MCM mice lacking the STX1A flox/flox with tamoxifen injections) were used to control for possible effects of tamoxifen, activated Cre, or the tamoxifen solvent (peanut oil). These mice showed no significant difference in heart function measured using echocardiography over the

monitoring period. The only deviation noted was in the software-generated CO in which control mice had a higher CO than Cre+ mice at 4 weeks post injections. TAM mice, which displayed a CO very close to that of the control mice, were not statistically different than the Cre+ mice. This single point can be explained by the way these parameters are estimated. During echocardiography, the only direct measurements done are those of the systolic and diastolic dimensions. The remaining parameters such as CO are generated using a built-in algorithm. Using these generated values alone fails to take into consideration the error in HR and SV, the product of which is CO. It is also worth noting that HR and SV at 4 weeks post injections were not significantly different. When calculating CO using these two values, and their associated errors, the significant difference at 4 weeks between control and Cre+ mice is no longer noted. The general pattern of the software-generated CO and the calculated CO are identical with the only difference being the compounded error now carried by the calculated CO values. Considering that the software-generated CO was seen to be significantly different between the control and Cre+ groups at a single point should not undermine the fact that at all time points before and after the 4^{th} week these groups were not statistically different.

4.4 Effect of STX1A Knockout on Heart Function

Prior to this thesis, the effect on heart function in cardiomyocyte-specific STX1A KO mice had not been explored. Upon visual inspection of the echocardiography M-modes, an evident decline in LV wall movement can be noted at 0-week post tamoxifen treatment. By week 3, the LV wall traces are similar to those of the pre-tamoxifen treatment condition. STX1A KO mice display elevated Ds, Vs, and reduced EF, and FS, indicative of temporary systolic

dysfunction. It has been established that the observed phenotype is not in response to other variables such as tamoxifen or Cre recombinase activity. Echocardiography also shows no change in HR, SV, and calculated CO. The abovementioned arguments explaining the differences between the software-generated and calculated CO also apply to the STX1A KO CO. Observations thus far, agree with each other at a systemic level and can be explained as following. STX1A KO hearts display increased Ds and Vs over the 0-3 week period. During this period, at 0- and 3-week post tamoxifen-treatment there is also a marginal but significant increase in Dd and Vd. Keeping HR, SV, and CO constant, increasing just Vs, and Vd can still produce reduced EF and FS, as shown by echocardiography data modeled in Table 2.

Table 2: A numerical illustration of the effect of STX1A KO on heart function. This theoretical situation models the observed treads during echocardiography following STX1A KO. The values used in this model for ejection fraction (EF) are values observed during data collection.

Cre+	STX1A KO	Change
SV = 5 µL	SV = 5 µL	Same
EF = 70%	EF = 40%	Reduced
Vs = 2.14 µL	Vs = 7.5 µL	Increased
Vd = 7.14 µL	Vd = 12.5 µL	Increased

Invasive hemodynamics indicate no change in afterload in STX1A as AoP during systole and diastole remain the same prior to and after tamoxifen administration. This rules out the phenotype being a secondary response to increased afterload and points towards a mechanism intrinsic to cardiomyocytes (Heineke and Molkentin 2006; Tarazi and Levy 1982). In addition, myocardial hypertrophy, which is very commonly associated with elevated afterload, is not seen in STX1A KO mice, as will be discussed later. Reduced pressure generation by the LV can also be predicted based on the systolic function reported by echocardiography, however, this was not

supported by invasive hemodynamic data. LVP during systole and diastole were not shown to differ following STX1A KO. At this point it is worth noting a potential drawback of this technique. Reduced LVP generation is accompanied by an increase in preload. As the heart is not isolated from the rest of the circulatory system, this increase in preload can give rise to masking effects that make it appear as if the myocardium itself is producing the same initial force. During dilated cardiomyopathy, even though there is an increase in Vs and Vd, as observed, LVPs can remain unchanged (Lindsey et al. 2018). Isolating the heart using an *ex vivo* perfusion system, along with this data, would allow for more concrete conclusions regarding changes in LVP generation in the absence of STX1A. Invasive hemodynamics also shows declined peak rate of pressure generation and relaxation (dP/dt systole and diastole) at week 0, indicative of a prolonged cardiac cycle and systolic dysfunction (Lindsey et al. 2018). The delay observed between the peak of the R-wave and onset of LV contraction also points towards a prolongation of the cardiac cycle. HR at this point was not seen to be decreased, as would be predicted. In fact, by 3 weeks, invasive hemodynamics suggests increased HR in STX1A KO mice. This was not observed in data collected using echocardiography. As a separate control group was not used in the hemodynamics experiments due to a shortage of available mice, it is harder to rule out potential effects on cardiac physiology given this technique's invasive nature (Lindsey et al. 2018).

As of yet, a mechanism pertaining to this phenotype has not been deduced, however, there are some hypotheses that warrant further investigation. The first being possible disruption in EC coupling and the second being reduced sarcoplasmic calcium stores due to leaky voltage-gated calcium channels. Reduced calcium gain through EC coupling or reduced sarcoplasmic

calcium stores is described to be fundamental in reduced contractility (Gomez et al. 1997; Roe et al. 2015). A reduction in calcium gain can result from spatial dissociation between voltage-gated calcium channels and ryanodine receptors leading to desynchronized calcium release from the sarcoplasmic reticulum. This spatial dissociation can lead to orphaned ryanodine receptors, which result in slower release of calcium and lower amplitude calcium currents, thereby reducing the rate and strength of contraction (Bers 2002; Fabiato 1983; Louch et al. 2010; Roe et al. 2015).This EC uncoupling could potentially result from the knockout of STX1A as this protein has been shown to directly interact with voltage-gated L-type calcium channels and form nano-clusters of dimers and trimers localized to the plasma membrane (Sajman et al 2017). Keeping in mind the traditional role of SNARE proteins and its interactions with other proteins, it can be proposed that STX1A is involved in trafficking and localizing voltage-gated L-type calcium channels to the sarcolemma in a manner which optimizes coupling with ryanodine receptors. Secondly, STX1A KO could give rise to leaky voltage-gated calcium channels, increasing resting cytosolic calcium levels (Fong et al. 1990). This spontaneous uncoordinated opening of voltage-gated calcium channels in the absence of STX1A could lead to reduction of sarcoplasmic calcium stores resulting in slower and weaker contractions (Gomez et al. 1997; Roe et al. 2015). Currently there is no evidence that supports or refutes this possibility. Evidently, further investigation is required to determine a molecular explanation for the observed phenotype.

4.5 No Compensatory Myocardial Hypertrophy in STX1A Knockout Hearts

A hallmark feature of cardiomyocytes in a failing heart is hypertrophy (Anversa et al. 1991; Izumiya et al. 2006). During cardiac hypertrophy, cardiomyocytes increase in overall

volume by either increasing in length and/or width in an effort to compensate for diminished heart function (Heineke and Molkentin 2006). In order to explore the possibility of compensatory myocardial hypertrophy as an explanation for the observed functional recovery in STX1A KO mice, LV posterior wall thickness and heart weight-to-tibia length ratios were determined. However, both parameters were unable to suggest the presence of hypertrophy. Specifically, LV posterior wall thickness remained the same, both within and between all groups, before and after receiving their respective treatments. Further, heart weight-to-tibia length ratios at 0- and 3-week post-tamoxifen in αMHC-MCM STX1A flox/flox mice were not significantly different than those mice that received peanut oil injections. Therefore, both LV posterior wall thickness and heart weight-to-tibia length suggest the absence of compensatory hypertrophy—thus this phenomenon cannot account for the recovered heart function in STX1A KO mice.

4.6 Possible SNARE Protein Compensation in STX1A Knockout Cardiomyocytes

Western blots were performed on SNARE proteins similar in function to STX1A in the heart, such as STX2, 3, and 4. These proteins also localize to the sarcolemma and could potentially perform the role of STX1A (Ferlito et al. 2010, Mandon et al. 2017). STX3 has been demonstrated to interact with voltage-gated calcium channels as well (Xie et al 2016). It was shown that STX3 co-precipitates with the α_1 pore-forming subunit of voltage-gated calcium channels. This is the same subunit which STX1A has been reported to bind when inhibiting currents through these channels (Arien et al. 2003). Xie and team (2016) noted that upon STX3 KO in INS-1 cells, there was significant increase in the observed calcium current amplitudes. Using selective channel blockers, the researchers attributed this increase in currents to L- and R-

type calcium channels. STX3, however, doesn't appear to interact with these channels the same way STX1A does via cysteines -271 and -272 as these amino acids are not conserved in the transmembrane domain of STX3. It has been proposed that STX3 interacts with and modulates channel currents through its cytosolic domain (Xie et al. 2016). Such interactions with voltage-gated channels have not been established for STX2 and 4 as a result, there is greater probability of STX3 being the protein responsible for the observed recovery in STX1A KO hearts (Bezprozvanny et al. 2000). The delay observed in recovery, with the assumption STX3 is responsible, could be explained by the preferential binding of STX3 for voltage-gated R-type calcium channels over L-type channels, which are preferentially bound by STX1A (Xie et al 2016). It was demonstrated that STX1A co-precipitated with $Ca_V1.3$ (L-type calcium channel) 2.3 times more than $Ca_V2.3$ (R- type calcium channel) whereas, for STX3 was 2.8 times more in favour of $Ca_V2.3$. Thus, STX3 might then require a longer period of time before sufficient amounts of vacated L-type channels can be bound and modulated as done by STX1A. To do so, there may also be compensatory increase in STX3 expression followed by a 'correcting' period. Western blots on STX 2 and 3 however, were unsuccessful in detecting these proteins preventing any further conclusions regarding their involvement in rescuing the observed phenotype through increased compensatory expression. Western blot and densitometry data on STX4 fail to show change in expression levels of this SNARE protein following STX1A KO. Considering the possible complications associated with the western blot technique as discussed earlier, further investigation is required into these SNARE proteins and their potential role in recovery to form appropriate conclusions.

Chapter Five: Concluding Remarks and Future Directions

Assessing heart function in cardiomyocyte-specific STX1A KO mice using echocardiography and invasive hemodynamics is indicative of a transient systolic dysfunction. Reduction in heart function is observed in the first 3 weeks following STX1A KO, which later returns to normal levels. From these observations, it can be proposed that STX1A somehow is involved in maintaining EC coupling efficiency and myocyte contractility. Further experimentation is required to deduce a mechanistic explanation on how STX1A performs this role in cardiomyocytes and the observed recovery in STX1A KO hearts. To do so, I recommend the following.

As western blots were unable to detect STX1A knockout, STX2, and 3, it is recommended that these blots be repeated using a new primary antibody. As previously discussed, crude lysate of freshly collected samples should be loaded to access and prevent possible loss of target protein during the removal of cellular debris while taking all precautions to minimize protein degradation (Ghosh et al. 2014; Murphy et al. 2009). In addition to this, reverse transcription quantitative polymerase chain reaction (RT-qPCR) to access expression levels of proteins involved in EC-coupling and candidate compensatory SNARE proteins, STX2, 3, 4 and their associated SNARE proteins SNAP-23/25 and VAMP-1/2 should be done. Ideally, a longitudinal assessment of transcript levels over a similar time frame as the echocardiography experiments should be done. In doing so, conclusions regarding changes in expression levels of these proteins in response to STX1A knockout and the observed cardiac function at that state can be used to further evaluate their purposed role in recovery.

It is suggested that additional control groups, such as Cre+ mice, be included in invasive hemodynamic experiments in order to rule out any external variables which may be influencing the trends reported in this thesis. *Ex vivo* heart perfusion experiments, also referred to as Langendorff method, should also be done to supplement hemodynamic data. These two experiments, being similar to one another, are not mutually exclusive (Lindsey et al. 2018). Performing isolated heart perfusion to assess LV pressure generation will allow ruling out of a possible masking effect of blood *in vitro* as discussed above.

Through the use of optical mapping, one can assess the proposed role of STX1A in EC coupling (Jaimes 3rd et al. 2016). Using high fidelity calcium-sensitive fluorescent probes, changes in calcium kinetics and amplitudes in cardiomyocytes can be measured at a considerably high resolution. The technique can also provide insight to potential spontaneous opening or leakiness of voltage-gated calcium channels as a result of STX1A knockout. Finally, whole-cell patch clamp, a commonly used but challenging technique, can be used to study voltage-gated calcium channel kinetics in STX1A knockout cardiomyocytes (Rubaiy 2017). This data, along with optical mapping, will allow further characterization of the role of STX1A in the heart.

References

Anversa, P., Olivetti, G., & Capasso, J. M. (1991). Cellular basis of ventricular remodeling after myocardial infarction. *The American Journal of Cardiology*, *68*(14), 7–16.

Arien, H., Wiser, O., Arkin, I. T., Leonov, H., & Atlas, D. (2003). Syntaxin 1A modulates the voltage-gated L-type calcium channel (Cavl.2) in a cooperative manner. *Journal of Biological Chemistry*, *278*(31), 29231–29239.

Asahi, M., Otsu, K., Nakayama, H., Hikoso, S., Takeda, T., Gramolini, A. O., MacLennan, D. H. (2004). Cardiac-specific overexpression of sarcolipin inhibits sarco(endo)plasmic reticulum Ca2+ ATPase (SERCA2a) activity and impairs cardiac function in mice. *Proceedings of the National Academy of Sciences of the United States of America*, *101*(25), 9199–9204.

Axelsson, J., Rippe, A., & Rippe, B. (2011). Transient and sustained increases in glomerular permeability following ANP infusion in rats. *American Journal of Physiology-Renal Physiology, 300*(1), F24-F30.

Barany, M. (1967). ATPase Activity of Myosin Correlated with Speed of Muscle Shortening. *The Journal of General Physiology*, *50*(6), 197-218.

Bers, D. M. (2002). Cardiac excitation–contraction coupling. *Nature*, *415*(6868), 198–205.

Bersell, K., Choudhury, S., Mollova, M., Polizzotti, B. D., Ganapathy, B., Walsh, S., Kuhn, B. (2013). Moderate and high amounts of tamoxifen in MHC-MerCreMer mice induce a DNA damage response, leading to heart failure and death. *Disease Models & Mechanisms*, *6*(6), 1459–1469.

Bezprozvanny, I., Zhong, P., Scheller, R. H., & Tsien, R. W. (2000). Molecular determinants of the functional interaction between syntaxin and N-type Ca2+ channel gating. *Proceedings of the National Academy of Sciences of the United States of America*, *97*(25), 13943–13948.

Bloch, K.D., Seidman, J.G., Naftilan, J.D., Fallon, J. T., Seidman, C. E. (1986). Neonatal atria and ventricles secrete atrial natriuretic factor via tissue-specific secretory pathways. *Cell*, *47*(5), 695-702.

Brose, N. (2014). All roads lead to neuroscience: The 2013 nobel prize in physiology or medicine. *Neuron*, *81*(4), 723–727.

Brown, J., & Corr, L. (1987). Renal mechanisms of human a-atrial natriuretic peptide in man. *The Journal of Physiology*, *387*, 31-46.

Buerger, A., Rozhitskaya, O., Sherwood, M. C., Dorfman, A. L., Bisping, E., Abel, E. D., Jay, P. Y. (2006). Dilated Cardiomyopathy Resulting From High-Level Myocardial Expression of Cre-Recombinase. *Journal of Cardiac Failure*, *12*(5), 392–398.

Chao, C., Liang, T., Kang, Y., Lin, X., Xie, H., Feng, Z.P., & Gaisano, H.Y. (2011). Syntaxin-1A inhibits KATP channels by interacting with specific conserved motifs within sulfonylurea receptor 2A. *Journal of Molecular and Cellular Cardiology*, *51*(5), 790-802.

Chen, Y. A., & Scheller, R. H. (2001). SNARE-mediated membrane fusion. *Nature Reviews Molecular Cell Biology*, *2*, 98–106.

Cheng, H., Lederer, W.J., & Cannell, M.B. (1993). Calcium sparks: elementary events underlying excitation-contraction coupling in heart muscle. *Science, 262*(5134), 740-744.

Chu, M., Gao, Y., Zhang, Y., Zhou, B., Wu, B., Yao, J., & Xu, D. (2015). The role of speckle tracking echocardiography in assessment of lipopolysaccharide-induced myocardial dysfunction in mice. *Journal of Thoracic Disease*, *7*(12), 2253–2261.

Colazzo, F., Castiglioni, L., Sironi, L., Fontana, L., Nobili, E., Franzosi, M., & Guerrini, U. (2015). Murine left atrium and left atrial appendage structure and function: Echocardiographic and morphologic evaluation. *PLoS ONE*, *10*(4), 1–21.

Crossman, D. J., Ruygrok, P. R., Soeller, C., & Cannell, M. B. (2011). Changes in the organization of excitation-contraction coupling structures in failing human heart. *PLoS ONE*, *6*(3).

Cuocolo, A., Volpe, M., Mele, A.F., Celentano, L., Neumann, R.D., Trimarco, B., & Salvatore, M. (1991). Effects of atrial natriuretic peptide on glomerular filtration rate in essential hypertension: a radionuclide study. *European Journal of Nuclear Medicine and Molecular Imaging, 18*(1), 32-37.

De Bold, A. J., Raymond, J.J., & Bencosme S. A. (1978). Atrial specific granules of the rat heart: light microscopic staining and histochemical reactions. *Journal of Histochemistry & Cytochemistry, 26*(12), 1094-1102.

De Bold, A.J., Borenstein, H.B., Veress, A.T., & Sonnenberg, H. (1981). A rapid and potent natriuretic response to intravenous injection of atrail myocardial extract in rats. *Life Sciences*, *28*(1), 89-94.

De Camilli, P., Cameron, R., & Greengard, P. (1983). Synapsin I (protein I), a nerve terminal-specific phosphoprotein. I. Its general distribution in synapses of the central and peripheral nervous system demonstrated by immunofluorescence in frozen and plastic sections. *Journal of Cell Biology*, *96*(5), 1337–1354.

De Waard, M. C., Van Der Velden, J., Bito, V., Ozdemir, S., Biesmans, L., Boontje, N. M., Duncker, D. J. (2007). Early exercise training normalizes myofilament function and attenuates left ventricular pump dysfunction in mice with a large myocardial infarction. *Circulation Research*, *100*(7), 1079–1088.

Duman, J.G. & Forte, J.G. (2003). What is the role of SNARE proteins in membrane fusion? *American Journal of Physiology-Cell Physiology, 285*(2), C237-C249.

Faber, G.M., Silva, J., Livshitz L., & Rudy Y. (2007). Kinetic Properties of the Cardiac L-Type Ca2+ Channel and Its Role in Myocyte Electrophysiology: A Theoretical Investigation. *Biophysical Journal*, *92*(5), 1522-1543.

Fabiato, A. (1983). Calcium-induce release of calcium from the cardiac sarcoplasmic reticulum. *American Journal of Physiology*, *245*(1), C1-C14.

Fan, Q., Huang, Z. M., Boucher, M., Shang, X., Zuo, L., Brinks, H., Gao, E. (2013). Inhibition of Fas-Associated Death Domain-Containing Protein (FADD) Protects against Myocardial Ischemia/Reperfusion Injury in a Heart Failure Mouse Model. *PLoS ONE*, *8*(9).

Fasshauer, D., Sutton, R.B., Brunger, A.T., & Jahn, R. (1998). Conserved structural features of the synaptic fusion complex: SNARE proteins reclassified and Q- and R-SNAREs. *Proceedings of the Natural Academy of Sciences of the United States of America*, *95*(26), 15781-15786.

Ferlito, M., Fulton, W. B., Zauher, A. M., Marban, E., Steenbergen, C., & Lowenstein, C. J. (2010). VAMP-1, VAMP-2 and Syntaxin-4 Regulate ANP Release from Cardiac Myocytes. *Journal of Molecular and Cellular Cardiology.*, *49*(5), 791–800.

Fong, P. Y., Turner, P. R., Denetclaw, W. F., & Steinhardt, R. A. (1990). Increased activity of calcium leak channels in myotubes of Duchenne human and mdx mouse origin. *Science*, *250*(4981), 673–676.

Fukushima, N., Matsuura, K., Akazawa, H., Honda, A., Nagai, T., Takahashi, T., Komuro, I. (2011). A crucial role of activin a-mediated growth hormone suppression in mouse and human heart failure. *PLoS ONE*, *6*(12).

Gao, S., Ho, D., Vatner, D. E., & Vatner, S. F. (2011). Echocardiography in Mice. *Current Protocols in Mouse Biology*, (973), 71–83.

Gerst, J. E. (1999). SNAREs and SNARE regulators in membrane fusion and exocytosis. *Cellular and Molecular Life Sciences*, *55*(5), 707–734.

Ghosh, R., Gilda, J. E., Gomes, A. V, & Biology, M. (2014). The necessity of and strategies for improving confidence in the accuracy of western blots. *Expert Review of Proteomics*, *11*(5), 549–560.

Giraudo, C. G., Eng, W. S., Melia, T. J., & Rothman, J. E. (2006). A clamping mechanism involved in SNARE-dependent exocytosis. *Science*, *313*(5787), 676-680.

Gomez, A. M., Valdivia, H. H., Cheng, H., Lederer, M. R., Santana, L. F., Cannell, M. B., Lederer, W. J. (1997). Defective Excitation-Contraction Coupling in Experimental Cardiac Hypertrophy and Heart Failure. *Science*, *276*(5313), 800–806.

Grafmuller, A., Shillcock, J., & Lipowsky, R. (2009). The Fusion of Membranes and Vesicles: Pathway and Energy Barriers from Dissipative Particle Dynamics. *Biophysical Journal*, *96*(7), 2658-2675.

Hall, M. E., Smith, G., Hall, J. E., & Stec, D. E. (2011). Systolic dysfunction in cardiac-specific ligand-inducible MerCreMer transgenic mice. *American Journal of Physiology-Heart and Circulatory Physiology*, *301*(1), H253–H260.

He, Y., Kang, Y., Leung, Y.-M., Xia, F., Gao, X., Xie, H., Tsushima, R. G. (2006). Modulation of Kv2.1 channel gating and TEA sensitivity by distinct domains of SNAP-25. *Biochemical Journal*, *396*(2), 363–369.

Heineke, J., & Molkentin, J. D. (2006). Regulation of cardiac hypertrophy by intracellular signalling pathways. *Nature Reviews Molecular Cell Biology*, *7*(8), 589–600.

Hougen, K., Aronsen, J. M., Stokke, M. K., Enger, U., Nygård, S., Andersson, K. B., Sjaastad, I. (2010). Cre-loxP DNA recombination is possible with only minimal unspecific transcriptional changes and without cardiomyopathy in Tg(αMHC-MerCreMer) mice. *American Journal of Physiology-Heart and Circulatory Physiology*, *299*(5), H1671–H1678.

Izumiya, Y., Shiojima, I., Sato, K., Sawyer, D. B., Colucci, W. S., & Walsh, K. (2006). Vascular endothelial growth factor blockade promotes the transition from compensatory cardiac hypertrophy to failure in response to pressure overload. *Hypertension*, *47*(5), 887–893.

Jacoby, C., Molojavyi, A., Flögel, U., Merx, M. W., Ding, Z., & Schrader, J. (2006). Direct comparison of magnetic resonance imaging and conductance microcatheter in the evaluation of left ventricular function in mice. *Basic Research in Cardiology*, *101*(1), 87–95.

Jahn, R., & Scheller, R. H. (2006). SNAREs- engines for membrane fusion. *Nature Reviews Molecular Cell Biology*, *7*(9), 631–643.

Jaimes 3rd, R., Walton, R. D., Pasdois, P., Bernus, O., Efimov, I. R., & Kay, M. W. (2016). A technical review of optical mapping of intracellular calcium within myocardial tissue. *American Journal of Physiology-Heart and Circulatory Physiology*, *310*(11), H1388–H1401.

Janssen, B. J. A., De Celle, T., Debets, J. J. M., Brouns, A. E., Callahan, M. F., & Smith, T. L. (2004). Effects of anesthetics on systemic hemodynamics in mice. *American Journal of Physiology-Heart and Circulatory Physiology*, *287*(4), H1618–H1624.

Joho, S., Ishizaka, S., Sievers, R., Foster, E., Simpson, P. C., & Grossman, W. (2006). Left ventricular pressure-volume relationship in conscious mice. *American Journal of Physiology-Heart and Circulatory Physiology*, *292*(1), H369–H377.

Kam, M. K. M., Lee, K. Y., Tam, P. K. H., & Lui, V. C. H. (2012). Generation of NSE-MerCreMer transgenic mice with tamoxifen inducible Cre activity in neurons. *PLoS ONE*, *7*(5).

Kelsey, L., Flenniken, A. M., Qu, D., Funnell, A. P. W., Pearson, R., Zhou, Y. Q., Adamson, S. L. (2013). ENU-induced Mutation in the DNA-binding Domain of KLF3 Reveals Important Roles for KLF3 in Cardiovascular Development and Function in Mice. *PLoS Genetics*, *9*(7).

Koitabashi, N., Bedja, D., Zaiman, A. L., Pinto, Y. M., Zhang, M., Gabrielson, K. L., Kassz, D. A. (2009). Avoidance of transient cardiomyopathy in Cardiomyocyte-targeted Tamoxifen-induced mercremer gene deletion models. *Circulation Research*, *105*(1), 12–15.

Lam, P. P. L., Leung, Y. M., Sheu, L., Ellis, J., Tsushima, R. G., Osborne, L. K., & Gaisano, H. Y. (2005). Transgenic mouse overexpressing syntaxin-1A as a diabetes model. *Diabetes*, *54*(9), 2744–2754.

Layland, J., Solaro, R. J., & Shah, A. M. (2005). Regulation of Cardiac Contractile Function by Troponin I phosphorylation. *Cardiovascular Research.*, *66*(1), 12-21.

Liang, T., Qin, T., Xie, L., Dolai, S., Zhu, D., Prentice, K.J., Wheeler, M., Kang, Y., Osborne, L., & Gaisano, H.Y. (2016). New roles of syntaxin-1A in insulin granule exocytosis and replenishment. *Journal of Biology Chemistry*, *292*(6), 2203-2216.

Lien, C.L., Wu, C., Mercer, B., Webb, R., Richardson, J.A., & Olson, E.N. (1999). Control of early cardiac-specific transcription of Nkx2-5 by a GATA-dependent enhancer. *Development 126*(1), 75-84.

Lindsey, M. L., Kassiri, Z., Virag, J. A. I., De Castro Brás, L. E., & Scherrer-Crosbie, M. (2018). Guidelines for measuring cardiac physiology in mice. *American Journal of Physiology - Heart and Circulatory Physiology*, *314*(4), H733–H752.

Louch, W. E., Sejersted, O. M., & Swift, F. (2010). There goes the neighborhood: Pathological alterations in T-tubule morphology and consequences for cardiomyocyte Ca2+ handling. *Journal of Biomedicine and Biotechnology*, *2010*, 1–17.

Ma, Y., Zhang, X., Bao, H., Mi, S., Cai, W., Yan, H., Hu, Z. (2012). Toll-like receptor (tlr) 2 and tlr4 differentially regulate doxorubicin induced cardiomyopathy in mice. *PLoS ONE*, *7*(7).

Mandon, B., Nielsen, S., Kishore, B. K., & Knepper, M. A. (2017). Expression of syntaxins in rat kidney. *American Journal of Physiology-Renal Physiology*, *273*(5), F718–F730.

McGrath, M.F., de Bold, M.L.K., de Bold, A.J. (2005). The endocrine function of the heart. *Trends in Endocrinology & Metabolism*, *16*(10), 469-477.

Mishima, T., Fujiwara, T., Sanada, M., Kofuji, T., Kanai-Azuma, M., & Akagawa, K. (2014). Syntaxin 1B, but not syntaxin 1A, is necessary for the regulation of synaptic vesicle exocytosis and of the readily releasable pool at central synapses. *PLoS ONE*, *9*(2).

Murphy, R. M., Mollica, J. P., & Lamb, G. D. (2009). Plasma membrane removal in rat skeletal muscle fibers reveals caveolin-3 hot-spots at the necks of transverse tubules. *Experimental Cell Research*, *315*(6), 1015–1028.

Muthuramu, I., Amin, R., Postnov, A., Mishra, M., Jacobs, F., Gheysens, O., De Geest, B. (2017). Coconut oil aggravates pressure overload-induced cardiomyopathy without inducing obesity, systemic insulin resistance, or cardiac steatosis. *International Journal of Molecular Sciences*, *18*(7).

Muthuramu, I., Jacobs, F., Singh, N., Gordts, S. C., & De Geest, B. (2013). Selective Homocysteine Lowering Gene Transfer Improves Infarct Healing, Attenuates Remodelling, and Enhances Diastolic Function after Myocardial Infarction in Mice. *PLoS ONE*, *8*(5).

Nghiem, M., Sohal, D. S., Kimball, T. R., Molkentin, J. D., Witt, S. A., Penninger, J. M., Crackower, M. A. (2007). Temporally Regulated and Tissue-Specific Gene Manipulations in the Adult and Embryonic Heart Using a Tamoxifen-Inducible Cre Protein. *Circulation Research*, *89*(1), 20–25.

Núñez-Santana, F. L., Oh, M. M., Antion, M. D., Lee, A., Hell, J. W., & Disterhoft, J. F. (2014). Surface L-type Ca2+ channel expression levels are increased in aged hippocampus. *Aging Cell*, *13*(1), 111–120.

Olson, E.N. (2006). Gene Regulatory Networks in the Evolution and Development of the Heart. *Science*, *313*(5795), 1922-1927.

Perry, S. V. (2001). Vertebrate Tropomyosin: Distribution, Properties and Function. *Journal of Muscle Research & Cell Motility*, *22*(1), 5-49.

Peters, C. G., Miller, D. F., & Giovannucci, D. R. (2006). Identification, localization and interaction of SNARE proteins in atrial cardiac myocytes. *Journal of Molecular and Cellular Cardiology*, *40*(3), 361–374.

Petty, K. J., Kokko, J. P., Marver, D. (1981). Secondary effect of aldosterone on Na-KATPase activity in the rabbit cortical collecting tubule. *Journal of Clinical Investigation*, *68*(6), 1545-1521.

Pillai, J. B., Gupta, M., Rajamohan, S. B., Lang, R., Raman, J., & Gupta, M. P. (2006). Poly(ADP-ribose) polymerase-1-deficient mice are protected from angiotensin II-induced cardiac hypertrophy. *American Journal of Physiology-Heart and Circulatory Physiology*, *291*(4), H1545–H1553.

Pleasant-Jenkins, D., Reese, C., Chinnakkannu, P., Kasiganesan, H., Tourkina, E., Hoffman, S., & Kuppuswamy, D. (2017). Reversal of maladaptive fibrosis and compromised ventricular function in the pressure overloaded heart by a caveolin-1 surrogate peptide. *Laboratory Investigation*, *97*(4), 370–382.

Popović, Z. B., Sun, J. P., Yamada, H., Drinko, J., Mauer, K., Greenberg, N. L., Thomas, J. D. (2005). Differences in left ventricular long-axis function from mice to humans follow allometric scaling to ventricular size. *Journal of Physiology*, *568*(1), 255–265.

Pugach, Ek., Richmond, P.A., Azofeifa, J.G., Dowell, R.D., & Leinwand, L.A. Prolonged Cre expression driven by the α-myosin heavy chain promoter can be cardiotoxic. *Journal of Molecular and Cellular Cardiology.* 86, 54-61 (2015).

Ramos-Vara, J. A. (2005). Technical aspects of immunohistochemistry. *Veterinary Pathology*, *42*(4), 405–426.

Ribatti, D. (2009). William Harvey and the discovery of the circulation of the blood. *Journal of Angiogenesis Research*, *1*, 3.

Roe, A., Frisk, M., & Louch, W. (2014). Targeting Cardiomyocyte Ca2+ Homeostasis in Heart Failure. *Current Pharmaceutical Design*, *21*(4), 431–448.

Rothman, J. E. (1994). Mechanisms of intracellular protein transport. *Nature*, *372*, 55–63.

Rubaiy, H. N. (2017). A short guide to electrophysiology and ion channels. *Journal of Pharmacy and Pharmaceutical Sciences*, 48–67.

Rubattu, S., Stanzione, R., Di Angelantonio, E., Zanda, B., Evangelista, A., Tarasi, D., Gigante, B., Pirisi, A., Brunetti, E., Volpe, M. (2004). Atrial natriuretic peptide gene polymorphisms and risk of ischemic stroke in humans. *Stroke*, *35*(4), 814-818.

Sajman, J., Trus, M., Atlas, D., & Sherman, E. (2017). The L-type Voltage-Gated Calcium Channel co-localizes with Syntaxin 1A in nano-clusters at the plasma membrane. *Scientific Reports*, *7*, 1–11.

Santana, L. F., Cheng, E. P., & Lederer, W. J. (2010). How does the shape of the cardiac action potential control calcium signaling and contraction in the heart? *Journal of Molecular and Cellular Cardiology*, *49*(6), 901–903.

Scales, S. J., Chen, Y. A., Yoo, B. Y., Patel, S. M., Doung, Y. C., & Scheller, R. H. (2000). SNAREs contribute to the specificity of membrane fusion. *Neuron*, *26*(2), 457–464.

Seidah, N.G., Lazure, C., Chrftien, M., Thibault, G., Garcia, R., Cantin, M., Genest, J., Nutt, R.F., Brady, S.F., Lyle, T.A., Paleveda, W.J., Colton, C.D., Ciccarone, T.M., Veber, D.F. (1984). Amino acid sequence of homologous rat atrial peptides: Natriuretic activity of native and synthetic forms. *Proceedings of the National Academy of Sciences of the United States of America, 81*(9), 2640-2644.

Seino, S. & Shibasaki, T. (2005). PKA-dependent and PKA-independent pathways for cAMP-regulated exocytosis. *Physiological Reviews*, *85*(4), 1303-1342.

Sheng, Z. H., Rettig, J., Cook, T., & Catterall, W. A. (1996). Calcium-dependent interaction of N-type calcium channels with the synaptic core complex. *Nature*, *379*(6564), 451–454.

Silverman, M.E. (2007). De Motu Cordis: the Lumleian Lecture of 1616 An imagined playlet concerning the discovery of the circulation of the blood by William Harvey. *Journal of the Royal Society of Medicine*, *100*(4). 199-204.

Sohal, D. S., Nghiem, M., Crackower, M. A., Witt, S. A., Kimball, T. R., Tymitz, K. M., Penninger, J. M., & Molkentin, J. D. (2001). Temporally regulated and tissue-specific gene manipulations in the adult and embryonic heart using a tamoxifen-inducible Cre protein. *Circulation Research*, *89*(1), 20-25.

Stephens, R. E. (1965). Analysis of Muscle Contraction by Ultraviolet Microbeam Disruption of Sarcomere Structure. *Journal of General Physiology*, *25*(2), 129-139.

Stephenson, T. J. (1990). Atrial natriuretic factor: the heart as an endocrine organ. *Archives of Disease in Childhood*, *65*, 1293-1294.

Tarazi, R. C., & Levy, M. N. (1982). Cardiac responses to increased afterload state-of-the-art review. *Hypertension*, *4*(3), 8–18.

Toft-Bertelsen, T. L., Ziomkiewicz, I., Houy, S., Pinheiro, P. S., & Sorensen, J. B. (2016). Regulation of Ca2+ channels by SNAP-25 via recruitment of syntaxin-1 from plasma membrane clusters. *Molecular Biology of the Cell*, *27*(21), 3329–3341.

Trivedi, C. M., Min, M. L., Wang, Q., & Epstein, J. A. (2008). Transgenic overexpression of Hdac3 in the heart produces increased postnatal cardiac myocyte proliferation but does not induce hypertrophy. *Journal of Biological Chemistry*, *283*(39), 26484–26489.

Ullrich, A., Böhme, M. A., Schöneberg, J., Depner, H., Sigrist, S. J., & Noé, F. (2015). Dynamical Organization of Syntaxin-1A at the Presynaptic Active Zone. *PLoS Computational Biology*, *11*(9), 1–22.

Ungar, D. & Hughson, F.M. (2003). SNARE protein structure and function. *Annual Review of Cell and Developmental Biology*,19, 493-517.

Watanabe, H., Yamashita, T., Saitoh, N., Kiyonaka, S., Iwamatsu, A., Campbell, K. P., Takahashi, T. (2010). Involvement of Ca2+ channel synprint site in synaptic vesicle endocytosis. *Journal of Neuroscience*, *30*(2), 655–660.

Weber, T., Zemelman, B.V., McNew, J.A., Westermann, B., Gmachl, M., Parlati, F., Söllner, T.H., & Rothman, J.E. (1998). SNAREpins: minimal machinery for membrane fusion. *Cell*, *92*(6), 759-772.

Wheeler, M., Gaisano, H. Y., Dolai, S., Prentice, K. J., Kang, Y., Qin, T., Liang, T. (2016). New Roles of Syntaxin-1A in Insulin Granule Exocytosis and Replenishment. *Journal of Biological Chemistry*, *292*(6), 2203–2216.

Wilkins, M.R., Redondo, J., & Brown, L.A. (1997). The natriuretic-peptide family. *The Lancet*, *349*(9061), 1307-1310.

Wiser, O., Bennett, M. K., & Atlas, D. (1996). Functional interaction of syntaxin and SNAP-25 with voltage-sensitive L- and N-type Ca2+ channels. *The EMBO Journal*, *15*(16), 4100–4110.

Wiser, O., Cohen, R., & Atlas, D. (2002). Ionic dependence of Ca2+ channel modulation by syntaxin 1A. *Proceedings of the National Academy of Sciences of the United States of America*, *99*(6), 3968-3973.

X. Zhao, D. Ho, S. Gao, C. Hull, D. E. Vatner, S. F. V. (2012). Arterial Pressure Monitoring in Mice. *Current Protocols in Mouse Biology.*, *1*(Table 1), 105–122.

Xie, L., Dolai, S., Kang, Y., Liang, T., Xie, H., Qin, T., Gaisano, H. Y. (2016). Syntaxin-3 binds and regulates both R- and L-type calcium channels in insulin-secreting INS-1 832/13 Cells. *PLoS ONE*, *11*(2), 1–13.

Yang, B., Larson, D. F., & Watson, R. (2017). Age-related left ventricular function in the mouse: analysis based on in vivo pressure-volume relationships. *American Journal of Physiology-Heart and Circulatory Physiology*, *277*(5), H1906–H1913.

Yue, T.L., Gu, J.L., Reith, A.D., Lee, J.C., Mirabile, R.C., Kreutz, R., Wang, Y., Maleef, B., Parsons, A.A., & Ohlstein, E.H. (2000). Extracellular signal-regulated kinase plays an essential role in hypertonic agonists, endothelin-1 and phenyleprine-induced cardiomyocyte hypertrophy. *The Journal of Biological Chemistry*, *275*(48), 37895-37901.

Zheng, L., Xu, J., Qiu, W., Liu, X., Zhao, C. M., Chen, D., & Chen, Y. (2010). Cardioprotection of exogenous erythropoietin in mice with ligature-induced aortic stenosis: Effects on maladaptive cardiac hypertrophy. *Journal of Physiology and Pharmacology*, *61*(1), 13–20.